

AD-A050 142

MAYO FOUNDATION ROCHESTER MINN DEPT OF PHYSIOLOGY AN--ETC F/6 6/16  
PROTECTION OF THE CARDIOPULMONARY SYSTEMS AGAINST THE INJURIOUS--ETC(U)  
NOV 77 P A CHEVALIER

F49620-76-C-0001

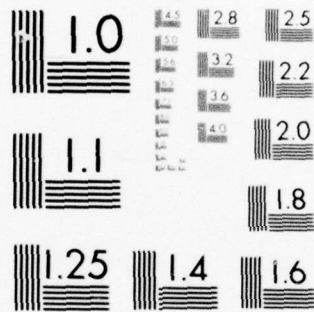
UNCLASSIFIED

AFOSR-TR-78-0102

NL

| OF |  
AD  
A050142





MICROCOPY RESOLUTION TEST CHART  
NATIONAL BUREAU OF STANDARDS-1963-A

SECURITY CLASSIFICATION OF THIS PAGE (When Data Entered)

# REPORT DOCUMENTATION PAGE

READ INSTRUCTIONS  
BEFORE COMPLETING FORM

1. REPORT NUMBER <b>AFOSR TR-78-0102</b>	2. GOVT ACCESSION NO.	3. RECIPIENT'S CATALOG NUMBER <b>progress</b>
4. TITLE (and Subtitle) <b>PROTECTION OF THE CARDIOPULMONARY SYSTEMS AGAINST THE INJURIOUS EFFECTS OF ACCELERATION</b>	5. TYPE OF REPORT & PERIOD COVERED <b>Final Scientific Report</b> <b>1 Jul 76 - 30 Sep 77</b>	
6. AUTHOR(s) <b>Peter A./Chevalier</b>	7. PERFORMING ORG. REPORT NUMBER	
8. CONTRACT OR GRANT NUMBER(s) <b>F49620-76-C-0001</b>	9. PROGRAM ELEMENT, PROJECT, TASK AREA & WORK UNIT NUMBERS <b>61102F</b> <b>2312/A2</b>	
10. PERFORMING ORGANIZATION NAME AND ADDRESS <b>Mayo Foundation</b> <b>Department of Physiology and Biophysics</b> <b>Rochester, Minnesota 55901</b>	11. REPORT DATE <b>23 Nov 1977</b>	
11. CONTROLLING OFFICE NAME AND ADDRESS <b>Air Force Office of Scientific Research (NL)</b> <b>Bolling AFB, DC 20332</b>	12. NUMBER OF PAGES <b>48</b>	
14. MONITORING AGENCY NAME & ADDRESS (if different from Controlling Office)	15. SECURITY CLASS. (of this report) <b>Unclassified</b>	
15a. DECLASSIFICATION/DOWNGRADING SCHEDULE		

16. DISTRIBUTION STATEMENT (of this Report) <b>Approved for public release; distribution unlimited.</b>
17. DISTRIBUTION STATEMENT (of the abstract entered in Block 20, if different from Report)
18. SUPPLEMENTARY NOTES
19. KEY WORDS (Continue on reverse side if necessary and identify by block number) <b>This report describes the</b> <b>which makes it possible</b>
20. ABSTRACT (Continue on reverse side if necessary and identify by block number) <b>The development of the parenchymal marker technique, as well as the ability to reconstruct three-dimensional shapes and dimensions of the heart, lung, chest-wall and diaphragm, in the intact thorax, presents a unique opportunity to study dynamic regional lung mechanics and lung-chest wall-diaphragm interaction under various conditions of lung volumes and body position and thereby provides the methodology to study the effects on regional lung function of alterations in these parameters induced by changes in the gravitational-inertial force</b>

**DDC**  
**RECEIVED**  
**FEB 17 1978**  
**ALBANY**  
**F**

DD FORM 1 JAN 73 1473 EDITION OF 1 NOV 65 IS OBSOLETE

UNCLASSIFIED

SECURITY CLASSIFICATION OF THIS PAGE (When Data Entered)

408 960 J05

AD A050142

DDC FILE COPY

UNCLASSIFIED

SECURITY CLASSIFICATION OF THIS PAGE(When Data Entered)

20. ~~Environment~~. Significant new information has been obtained regarding regional mechanical properties of the lung with techniques possessing sufficient temporal and spatial resolution to permit quantitative determination of the dynamic changes in spatial (three-dimensional) lung parenchymal strains, regional lung volumes and lung-chest wall geometries. <sup>Such</sup> Mechanical studies of the intact lung have ~~(therefore)~~ not been possible. These <sup>new</sup> results, which cannot be obtained by other methods, provide a quantitative measure of the mechanical properties of the lung under normal physiologic conditions (i. e., an intact thorax and normal intrathoracic pressures) at 1G and are required before ~~any~~ similar studies can be performed under conditions of increased or decreased gravitational-inertial force environments encountered in aerospace flight.

X

ACTIVITY	✓
REVIEW	✓
APPROVAL	✓
DISTRIBUTION/AVAILABILITY CODES	
1/1	SPECIAL
A	-

UNCLASSIFIED

SECURITY CLASSIFICATION OF THIS PAGE(When Data Entered)



Final Progress Report (July 1, 1976 - September 30, 1977)

Contract No. F49620-76-C-0001

Purchase Request No. 7T-0031

PROTECTION OF THE CARDIOPULMONARY SYSTEMS AGAINST THE INJURIOUS  
EFFECTS OF ACCELERATION

Evaluation of effects of time history of gravitational-inertial force environment on regional dynamic distribution of pulmonary ventilation, strains, edema and blood volume.

Introduction

Under dynamic conditions, the mechanical properties of the lung, rib cage, diaphragm, and abdomen and the coupling between these various components of the respiratory system, play an important role in determining the intrapulmonary distribution of inspired gas. It is known that the intrapulmonary distribution of inspired gas is altered by such factors as 1) body position, 2) lung volume, 3) chest wall geometry and compliance, and 4) increased gravitational-inertial force environments. In addition, slippage of lobes along interlobar fissures might aid the lung in conforming to differing thoraco-abdominal configurations without compromising regional ventilation, particularly during postural changes and exposure to increased gravitational-inertial force environments.

Because of the very fragile anatomic structure of the lungs and the large intrathoracic pressure differentials generated by changes in the force environment due to the extreme differences in specific gravity of the gaseous contents of the alveoli and the parenchyma and blood surrounding these alveoli, the lungs are the most susceptible organ system in the body to malfunction and structural

injury due to acceleration. Furthermore, it is quite possible that the regional distribution of mechanical stress within the lung is a predisposing factor in the localization of pulmonary pathology. Therefore, a quantitative description of the dynamic spatial distribution of lung parenchymal stresses and strains and the associated changes in dynamic shape and dimensions (i.e., the dynamic geometry) of the intact lungs and thorax is required before further progress can be made in describing the three-dimensional mechanical behavior of the intact lung. However, elucidation of the intrinsic elastic behavior of the lung and its relationship to the chest wall and diaphragm require studies of the intact lung with techniques possessing sufficient temporal and spatial resolution to permit quantitative measurements of the dynamic changes in the three-dimensional parenchymal stresses and strains, regional lung volumes, and thoracic shape and dimensions along with simultaneous measurements of transpulmonary and intravascular pressures.

This final progress report for Contract No. F49620-76-C-0001, covering the period July 1, 1976 to September 30, 1977, consists of three parts. Parts I and II contain summaries of individual studies performed during the period stated above and Part III consists of a list of publications from our laboratory which were based on work supported by funds from this contract.

Part I: Regional Parenchymal Expansion and Lung Mechanics in the Intact Canine Thorax from Measurements of the Displacements of Roentgenopaque Parenchymal Markers in Anesthetized Dogs

Experimental Preparation. Regional lung parenchymal expansion in the intact thorax can be determined by recording the displacements of radiopaque metallic markers by means of computer-based biplane roentgen-videographic recording system which provides high temporal

(30/sec) and spatial ( $\pm 1.0$  mm) resolution measurements of the "tagged" lungs (2). Metallic markers, which consist of 1-mm-diameter spheres (average weight: 0.01 gm/marker) and 2-mm-long (1-mm-diameter) rods (average weight: 0.02 gm/marker), were implanted percutaneously under fluoroscopic control throughout the parenchyma of the right lung of anesthetized dogs. A three-dimensional grid-like array of 30-40 markers (Figure 1) is obtained without causing physiologically significant pneumo- or hemothorax (2,8). A minimal recovery period of 2 to 3 weeks is provided before the dogs are used in an experiment. Then, by means of the biplane videoroentgenographic system, it is possible to continuously track the displacements, in three-dimensional space, of these radiopaque parenchymal markers throughout a complete respiratory cycle or maneuver (e.g., a static pressure-volume curve).

**DORSAL-VENTRAL AND LATERAL X-RAYS OF DOG'S  
THORAX WITH LUNG PARENCHYMAL MARKERS**

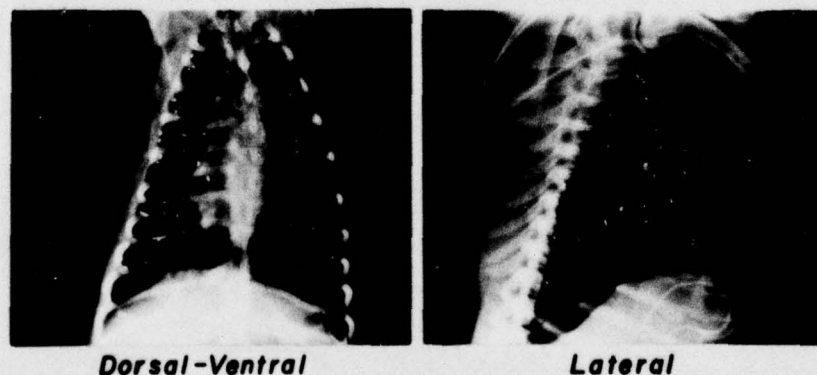


**Figure 1** Dorsal-ventral and lateral x-rays of dog's thorax with metallic markers percutaneously implanted in a three-dimensional grid-like array throughout the parenchyma of the right lung.

**Data Acquisition.** A schematic diagram of the biplane roentgen-videographic system and recording equipment used to quantitate the dynamic displacements of lung parenchymal markers during various



respiratory maneuvers is shown in Figure 2. Each roentgen-video imaging chain consists of an x-ray source, a 9-inch-diameter fluoroscopic screen and image-intensifier, and a television (Plumbicon) camera. The central axes of the two roentgen-video imaging systems can be selectively aligned from approximately 25-30° (i.e., the angle of separation of the imaging chain central axes) for stereo recording to 90° for orthogonal recording. The central axes of the two imaging systems are aligned so as to lie in the same transverse plane relative to the cephalocaudal axis of the animal and the animal is positioned so that the lungs and thorax are centered at the intersection of the axes of the roentgen-video imaging chains.

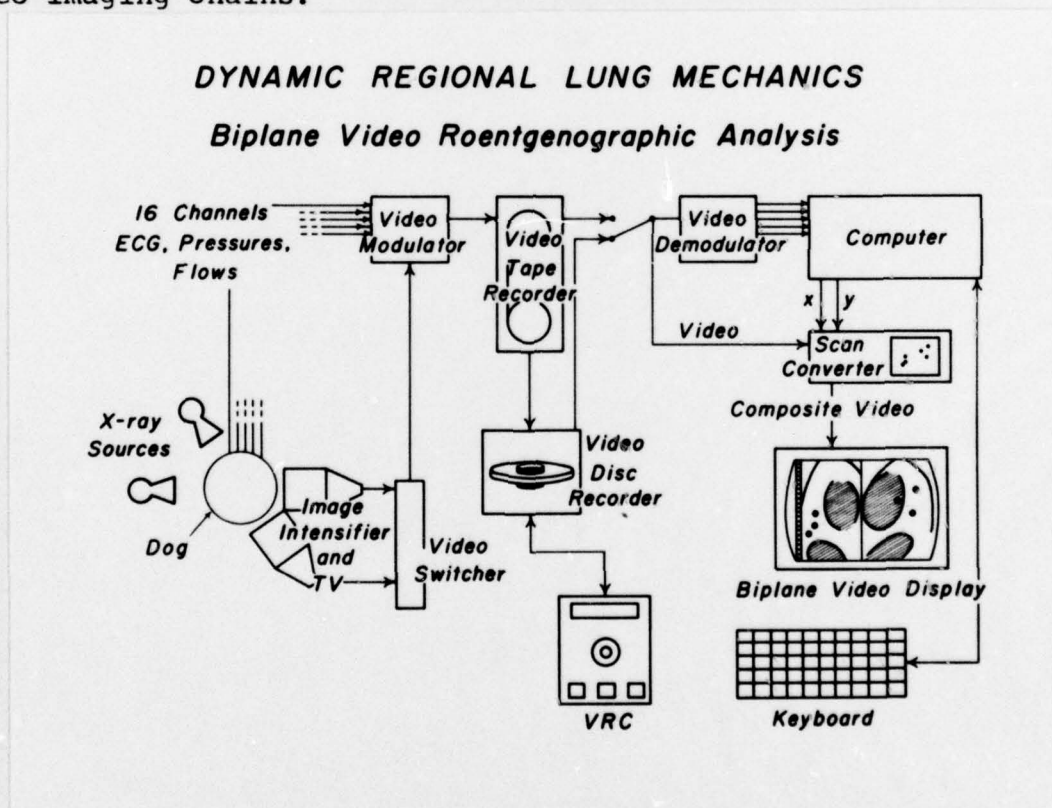


**Figure 2** Diagram of biplane roentgen-videographic system for generation and recording of data for dynamic measurements of regional lung strains and volumes. Axes of the two x-ray-video recording systems can be selectively aligned for stereo (as shown) or orthogonal recordings. Roentgen-video images and analog variables (pressures, flows, ECG) are simultaneously recorded on videotape or disc.

The fluoroscopic image which is projected onto the target of the television camera is recorded as a sequence of approximately 250 horizontal lines (1 video field; 1/60th sec) which is interlaced with a second field of as many lines to create a frame every 1/30th of a second containing approximately 500 lines per image. Then by means of special switching circuitry (10), the two video fields are positioned in the left and right halves of the video picture so that biplane videographic images are displayed and recorded simultaneously in the same video field. The sequence of 30/sec biplane images are recorded on videotape (Ampex VR 1100) in absolute temporal synchrony with up to 16 channels of analog information, such as vascular, pleural and airway pressures, velocity and volume of ventilation and the electrocardiogram (ECG) at sampling rates up to approximately 1000 samples/sec per analog channel by means of a video amplitude modulator-demodulator system (9).

At the end of an experiment, pressure, volume and flow calibrations and the reference (x,y,z) axes used for spatial localization of the markers are recorded on videotape. The reference axes are obtained by placing precision-milled 1-cm metal grids on the face of each image intensifier such that the centers of the two grids form a locus with spatial coordinates (0,0,0) to serve as the center of the cartesian reference system.

The geometry of the roentgen-video imaging systems can be arranged to accommodate 1) anesthetized dogs supported either head-up or head-down in a vertically-oriented radiolucent water-immersion respirator (2), 2) awake dogs standing in a Pavlovian-type sling positioned on the fluoroscopic table top for studies in spontaneously breathing awake animals (1), and 3) awake or anesthetized dogs breathing spontaneously in a horizontally-oriented, radiolucent, air-filled, plethysmograph (Figure 3) for continuous measurement of lung volumes and flows.



Data Processing and Analysis. Analysis of the biplane video images and multichannel analog recordings is accomplished by transferring the images from videotape to a stop-action video disc recorder (Ampex DR-10A) for frame-by-frame identification of parenchymal marker positions. A specially-designed computer station (Figure 2; lower right corner) consisting primarily of 1) an alphanumeric keyboard, to communicate with the computer, 2) an interactive video cursor which is "mixed" with the video image thereby eliminating parallax, 3) a video disc controller (VRC), and 4) a high performance video monitor (Tektronix 632), is used by an operator to track all parenchymal markers which are individually identifiable on both images of a single biplane video frame. Once the geometric coordinates of all parenchymal markers have been entered into computer memory, the operator directs the computer via the keyboard to transfer the coordinates and the analog data (pressures, flows, ECG) recorded with that video image from core memory to digital magnetic tape.

This regimen is then repeated on a frame-by-frame basis, for any selected time interval (i.e., time between frames analyzed), over the duration of the respiratory maneuver. In this way, the dynamic displacements, in three-dimensional space, of the parenchymal markers during various respiratory maneuvers can be determined with sufficient temporal (30/sec) and spatial ( $\pm 1.0$  mm) resolution to permit quantitation of regional lung parenchymal displacements and volumes in the intact thorax.

Experimental Procedure. Adult mongrel dogs, weighing 8-14 kg with parenchymal markers implanted previously, were used for these studies. The dogs were anesthetized with sodium pentobarbital (30 mg/kg I.V.) and a cuffed endotracheal tube was inserted into the airway. Intermittent positive-pressure breathing (end-inspiratory airway pressure, 10-15 cm H<sub>2</sub>O) was maintained with a Bird respirator (Bird Oxygen Breathing Equipment, Inc., Palm Springs, CA). Esophageal pressure ( $P_{es}$ ) was measured with a latex balloon positioned, under fluoroscopic

control, in the middle third of the esophagus. Transpulmonary pressure ( $P_{tp}$ ) was determined by subtracting airway ( $P_{aw}$ ), i.e., tracheal, pressure from  $P_{es}$  (5) by means of special electronic circuitry. The electrocardiogram (ECG) was also recorded. An indwelling catheter was inserted into the cephalic vein of the fore leg so that additional anesthetic could be given intravenously without opening the plethysmograph and disrupting the measurements.

The dog was then positioned in the plethysmograph (Figure 3), in either the prone or supine position, and all pressure and intravascular catheters, along with the ECG leads, were exteriorized through air-tight ports. The plethysmograph was closed, sealed and then aligned in the biplane roentgen-video imaging system (Figure 3). The animals breathed through a pneumotachograph (Fleisch #1, Dynasciences Medical Products, Blue Bell, PA) to measure velocity of air flow and volume (integral of flow velocity) of air moved during various respiratory maneuvers. Airway ( $P_{aw}$ ) and transpulmonary ( $P_{tp}$ ) pressures, velocity and volume of air flow and ECG are recorded on videotape and, with the exception of the ECG, on a 4-channel oscillographic recorder (Model 7414A, Hewlett-Packard Co., Palo Alto, CA). Validyne differential transducers, used to record airway (DP-9), and esophageal (DP-9) pressures and the pressure drop across the pneumotachograph (MP 45-2) were each interfaced with the oscillographic recorder via carrier amplifiers (CD-19, Validyne Engineering Corporation, Northridge, CA).

Static pressure-volume (P-V) curves were obtained for the intact and excised lungs by, starting from functional residual capacity (FRC) ( $P_{tp} = 2 \text{ H}_2\text{O}$ ), manually inflating the lungs with a calibrated 1000-ml-syringe in a step-wise manner (usually 100 ml/volume step) to total lung capacity (TLC) ( $P_{tp} = 25 \text{ cm H}_2\text{O}$ ) and then deflating in the same incremental manner back to FRC. Care is taken to impose the same volume history on the lungs immediately prior to doing the P-V maneuvers.

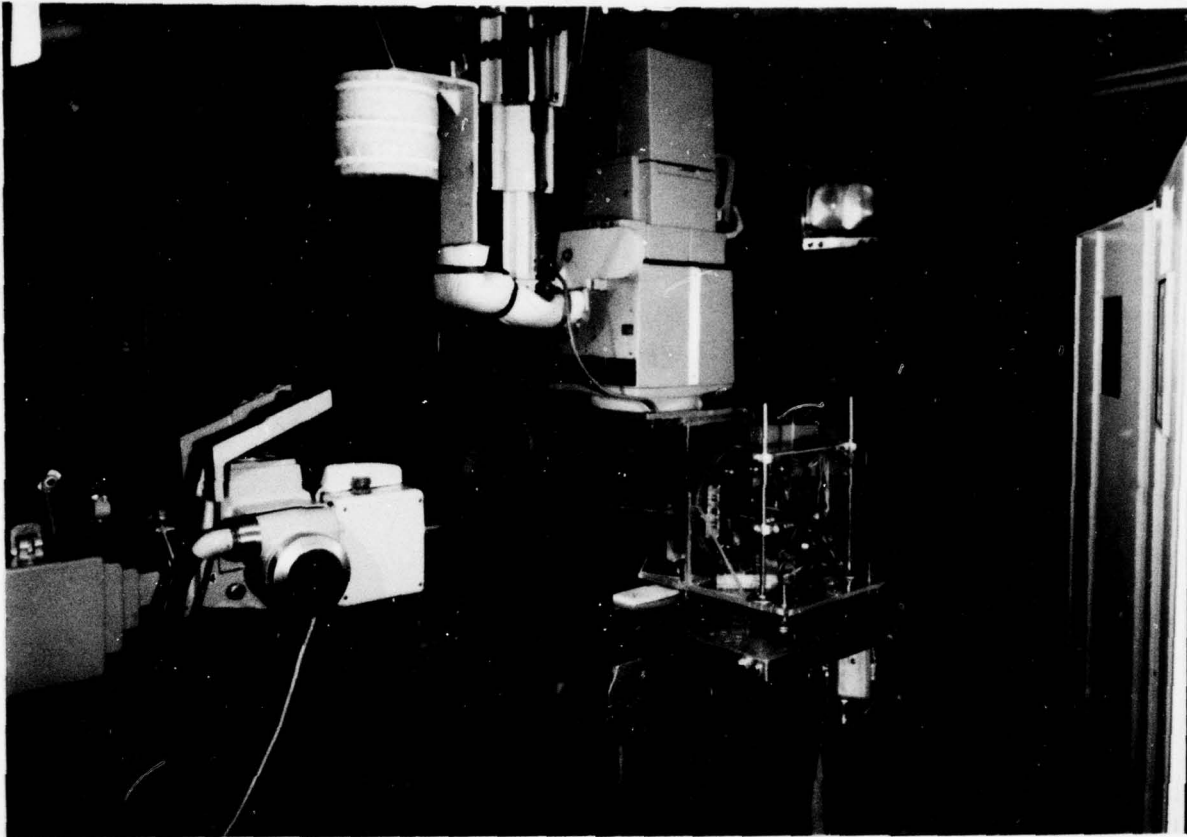


Figure 3 Cylindrical, air-conditioned, radiolucent body plethysmograph positioned in the biplane video-roentgenographic recording system. Plethysmograph permits quantitation of lung volumes and can be used with anesthetized spontaneously breathing or ventilated dogs in various positions (prone, supine, right and left lateral decubitus).

A. Effect of Cardiogenic Motion on Intermarker Distance Measurements.

The parenchymal markers are essentially randomly distributed throughout the right lung and hence, some are in closer proximity to the heart than others. It is quite evident from viewing recordings of different respiratory maneuvers, that parenchymal markers located near the heart undergo additional (i.e., unrelated to changes in lung volume) oscillation and displacement due to cardiogenic motion. This "cardiogenic" contribution to regional parenchymal marker displacement is observable at all lung volumes but its magnitude increases as lung volume decreases, i.e., as the lung



becomes less stiff. From the physiologic standpoint, studies indicate that this cardiogenic motion contributes to gas mixing in the lung and thereby reduces anatomic dead space (3,4).

To study the effect of cardiogenic motion on regional parenchymal marker displacements and intermarker distance measurements, an anesthetized prone dog was passively inflated in a step-wise manner from FRC to TLC and deflated back to FRC. Biplane roentgen-video images of this P-V maneuver were recorded on videotape, transferred to a stop-action video disc, and the geometric positions of the markers were determined, as described above, by two trained operators, each repeating the process three times.

Initially, marker positions were determined at each lung volume without regard to the phase of the cardiac cycle at which the measurements were made. Figure 4 (upper-half) shows the variability (i.e., standard deviation) of the intermarker distances as a function of mean intermarker distance. Data is based on six determinations of intermarker distances between 4 marker-pairs at each of 15 lung volumes ( $N = 60$ ). Note the small standard deviation (SD) of the intermarker distance measurements between markers close together (15-25 mm) in contrast to the relatively larger SD of the measurements of distance between markers further apart (35-60 mm). The reason for this is that the effect of cardiac motion on marker position diminishes with increasing distance of the marker from the heart. For marker-pairs which are near the heart, cardiogenic motion appears to displace each marker approximately equally and thus the distance between this marker-pair is little influenced by the beating heart. Similarly, for marker-pairs which are close together, but distant from the heart, intermarker distances do not appear to be influenced by cardiogenic motion due to the limited transmission of this motion through the lung parenchyma. On the other hand, for markers further apart such that one is near the heart and one is relatively distant from the heart, there is a greater effect of cardiac motion on intermarker distance measurements.

EFFECT OF CARDIOGENIC MOTION ON ACCURACY  
OF INTERMARKER DISTANCE MEASUREMENTS  
(6 Trials, 2 Observers)

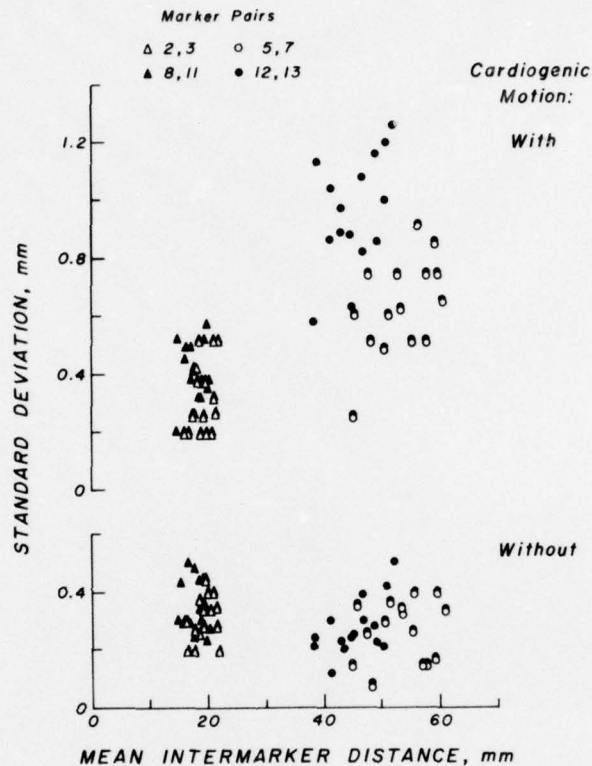


Figure 4 Effect of cardiogenic motion on intermarker distance measurements. Top-half: SD of intermarker distance measurements as a function of mean intermarker distance. Data based on 6 determinations of intermarker distances of 4 marker-pairs at each of 15 lung volumes (N = 60) without regard to phase of cardiac cycle. Bottom half: Similar plot obtained when marker positions were determined for each volume at the same point in the cardiac cycle.

Figure 4 (lower-half) is a similar plot obtained when the positions of the same markers were determined in the same manner as described above, but at identical points in the cardiac cycle. Note the



reduction in variability of the intermarker distance measurements. There is no longer any effect of intermarker distances on reproducibility. When cardiogenic motion is taken into account, the largest coefficient of variation observed was  $< 3\%$  for a marker pair separated by 16.5 mm. It is important to note that movement of the animal per se does not affect the measurements made with this technique since intermarker distances (i.e., distance between markers in three-dimensional space) are computed rather than displacements of markers from some fixed coordinate origin.

Figure 5 shows the frequency distribution of the maximum differences in intermarker distance measurements observed out of the 6 determinations for each of the 4 marker-pairs at the 15 volumes examined. The maximum difference in computed intermarker distance was less than 0.7 mm in 50% of the observations and was less than 1.0 mm in 80% of the observations. Since these measurements can be made as frequently as 30 times per second, this biplane roentgen-video-graphic technique is capable of providing temporal and spatial resolutions which are many-fold greater than that obtainable with radioactive gas (e.g.,  $^{133}\text{Xenon}$ ) techniques for measuring regional lung volumes.

The data presented in Figures 4 and 5 were obtained from a static pressure-volume maneuver, i.e., a step-wise inflation-deflation from FRC to TLC and back to FRC. From such a procedure, it is possible to plot a pressure-volume curve which provides limited information regarding the overall mechanical characteristics of the lung in the intact thorax. Since the biplane roentgen-video-graphic technique is capable of accurately determining the spatial, i.e., the three-dimensional, coordinates of each parenchymal marker, it is possible to construct regional pressure-intermarker distance curves for different lung regions. Figure 6 shows two such curves for marker-pairs located in the upper (marker pair 2,3) and lower

MAXIMUM DIFFERENCES IN INTERMARKER  
DISTANCES MEASURED BY 2 OBSERVERS  
(6 Trials, 4 Marker-Pairs,  
Intact Canine Lung,  $n = 60$ )

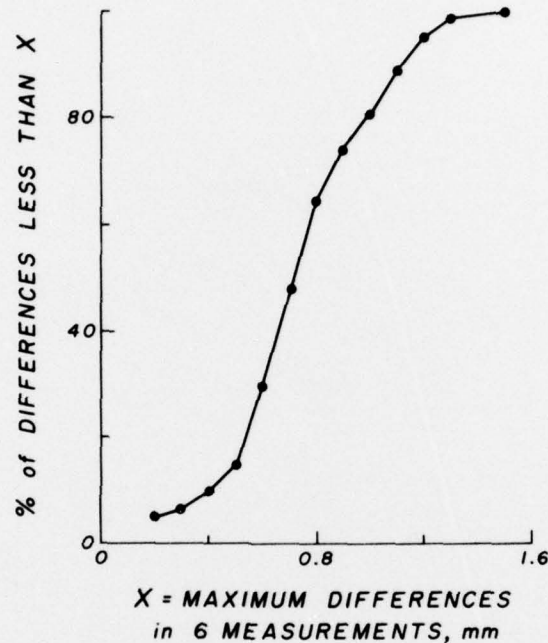


**Figure 5** A plot of the frequency distribution of the maximum differences in intermarker distance measurements obtained by 2 operators (3 trials each) using an operator-interactive, computer-generated video cursor to identify the spatial coordinates of 8 markers at each of 15 volumes ( $N = 60$ ) during a static pressure-volume maneuver. Measurements at each lung volume were made at the same point in the cardiac cycle.

(marker pair 5,7) regions of the right upper lobe of the intact canine lung. The data are the means  $\pm$  SD of 6 separate determinations by 2 operators (3 trials each) for the two marker-pairs at each of 15 lung volumes. The variability (i.e., SD) of these

measurements is quite small as evidenced by the vertical (SD) bars. Note also the hysteresis between the inflation (●) and deflation (○) portions of the maneuver as is seen in the conventional whole lung P-V curve.

If the lung expanded in a uniform or isotropic manner, i.e., for a given change in stress (transpulmonary pressure), the fractional elongation of the lung parenchyma along the x, y, and z axes was equivalent, it would be possible to calculate the spatial distribution of changes in regional lung volumes by simply cubing the distances between marker-pairs located in the various regions of the lung. However, it has been shown that lung expansion is not isotropic and that strains measured between two markers will depend on the spatial orientation of the markers within the lung parenchyma (2). Hence, pairs of markers can be used to quantitate inter- and intralobar strains, but cannot be used to calculate dynamic changes in regional lung volume (i.e., ventilation). However, the latter can be quantitated by selecting sets of 4 non-coplanar markers, with any given set of four contained within the same lobe, to define the vertices of a tetrahedron. Then by simply calculating the volume of each tetrahedron directly from solid geometry, the spatial and temporal distributions of changes in regional lung volume, relative to the lung itself (in contrast to inspired radioactive gas techniques) can be obtained throughout a respiratory maneuver. The dynamic changes in relative position of the markers, and hence the volume described by them, can then be further analyzed by well-established methods in mechanics (e.g., the affine transformation). Software to implement the affine transformation has recently become operational and initial results are currently being analyzed.



INTERMARKER DISTANCE - PRESSURE  
CURVES FOR INTACT CANINE LUNG  
(6 Trials, 2 Observers)

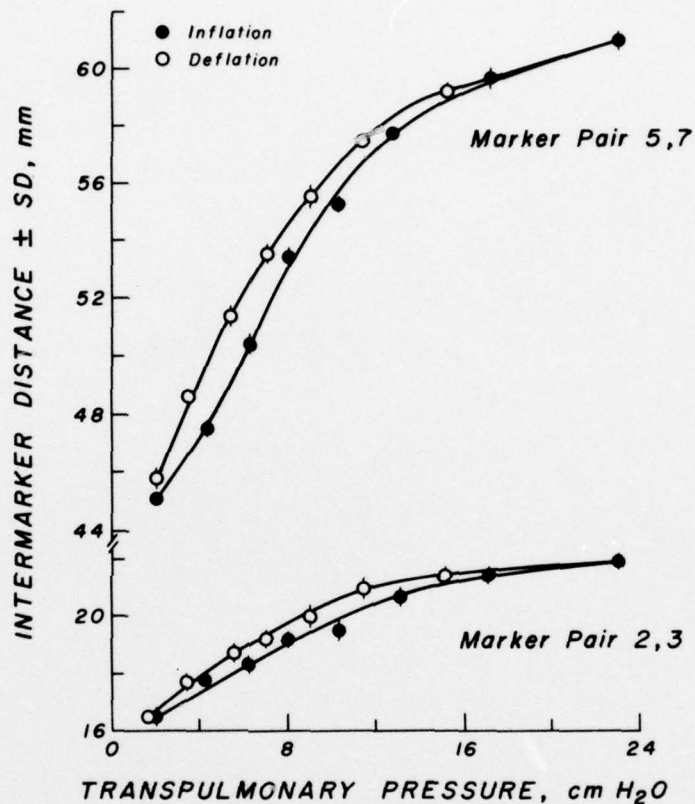


Figure 6 Intermarker distance - transpulmonary pressure curves obtained for the intact canine lung. Intermarker distance measurements represent the means  $\pm$  SD of 6 separate determinations by 2 operators (3 trials each) during a static pressure-volume maneuver. Measurements at each lung volume were made at the same point in the cardiac cycle.

B. Regional lung expansion in the intact vs. excised canine lung at TLC. To analyze regional lung deformation with the goal being to delineate the factors responsible for nonuniform ventilation, it is important to know if, at total lung capacity

(TLC), the lung, in the intact thorax, is deformed from its shape under conditions of uniform or isotropic expansion. Studies of dog lungs quick frozen at high inflation pressures reveal no systematic regional differences in alveolar size (6,7). This suggests that at TLC the lung is uniformly expanded.

To compare regional lung expansion in the intact and excised lung at TLC, we selected four dogs with good three-dimensional distributions of parenchymal markers. Static pressure-volume curves were obtained for the intact lungs by placing the dogs in the plethysmograph (Figure 3) in the prone position and inflating the lungs in a step-wise manner from FRC to TLC and then deflating in the same incremental manner back to FRC. The animals were then sacrificed and exsanguinated and the lungs were excised through a median sternotomy. No pleural adhesions were encountered in any of the animals studied. The entire excised lung was then returned to the plethysmograph and placed in the sling in as close to the same geometric orientation as it assumed in the intact prone animal as was possible. Static P-V curves were again obtained by inflating the lung from FRC ( $P_{tp} = 2.5 \text{ cm H}_2\text{O}$ ) to TLC ( $P_{tp} = 25 \text{ cm H}_2\text{O}$ ) and then deflating back to  $P_{tp} = 2.5 \text{ cm H}_2\text{O}$  in a step-wise manner. Biplane roentgen-video images of these maneuvers were recorded on videotape and the distances between all intralobar marker-pairs were determined at total lung capacity, as described above.

The results from the four dogs are shown in Figures 7 and 8. The distances between all intralobar marker-pairs at TLC are plotted for the intact prone dog (ordinate) versus the excised lung (abscissa) at the same inflation pressure. A good correlation (range:  $r = 0.966$  to  $0.999$ ) and a high degree of linearity of the distances between intralobar marker-pairs located in all three lobes of right lung, intact and excised, was observed. Note that the regression line is very close to the line of identity. Since the markers were essentially randomly distributed in the lung parenchyma, this



significant linear correlation indicates that the relationships of intralobar intermarker distances, in the intact and excised lung, was independent of spatial orientation and location within the lung. The close correspondence between intralobar intermarker distances indicates that each lobe was not only at the same volume but was expanded in an identical manner intact and excised. Assuming that at TLC, i.e., at high inflation pressures, the excised lung is stiff enough not to be deformed by its own weight, the lung should be uniformly or isotropically expanded. Therefore, changes in regional parenchymal shape and dimensions from that pertaining at TLC represent changes from the state of uniform expansion.

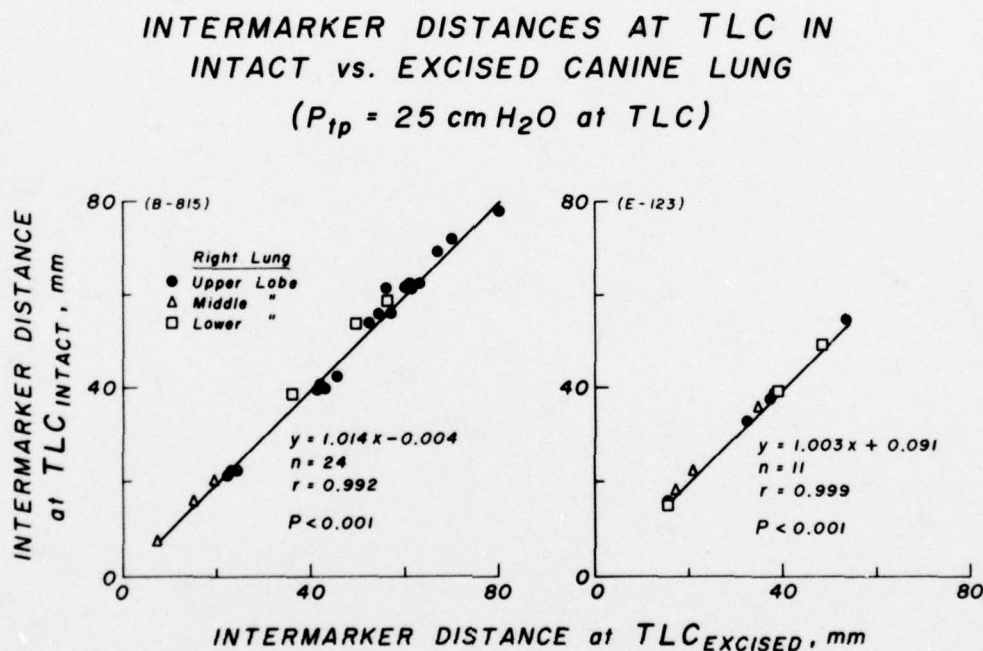


**Figure 7** Comparison of distances between intralobar marker-pairs in the right lung of 2 dogs at total lung capacity (TLC) with the lungs in the intact thorax (ordinate) and excised (abscissa).

**INTERMARKER DISTANCE AT TLC IN  
INTACT vs. EXCISED CANINE LUNG  
( $P_{tp} = 25 \text{ cm H}_2\text{O}$  at TLC)**

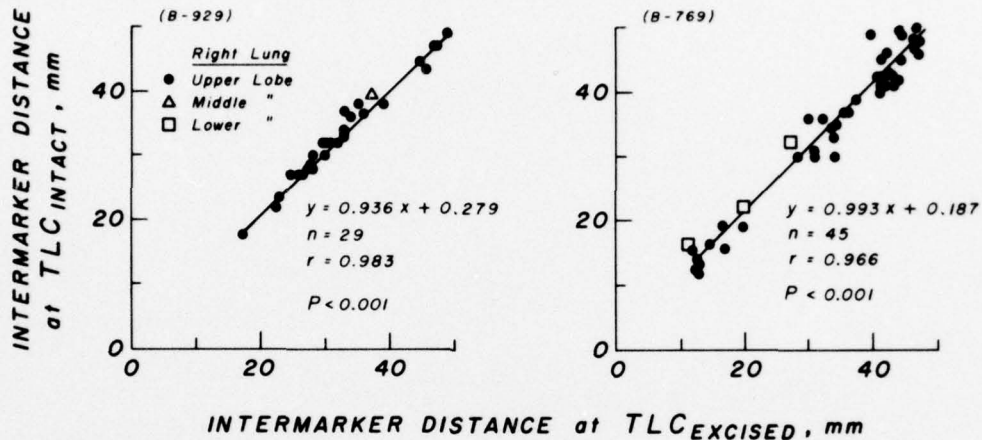
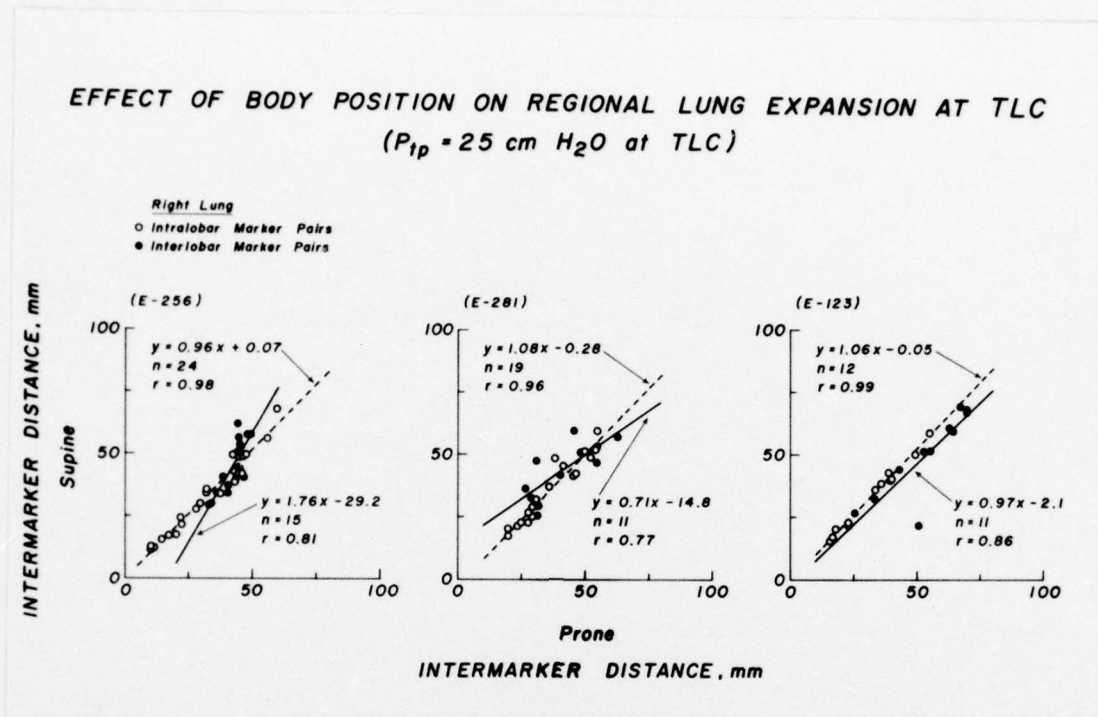


Figure 8 Similar to Figure 7 for 2 additional dogs.

C. Regional lung expansion at TLC in the intact thorax in the prone and supine positions. A similar series of experiments were performed in intact anesthetized dogs in the prone and supine body positions. Three dogs, with good three-dimensional marker distributions, were used for this study, one of which (E-123) was used in both studies. Each dog was anesthetized and positioned in the plethysmograph in the prone and supine positions and pressure-volume maneuvers were performed, as described above, in both positions for each animal. The results from the three dogs are shown in Figure 9. The distances between all intralobar marker-pairs were determined at TLC ( $P_{tp} = 25 \text{ cm H}_2\text{O}$ ) and compared when the animals were in the supine (ordinate) versus prone (abscissa) position. Again, there is a significant linear correlation (range:  $r = 0.96$  to  $0.99$ ) of distances between intralobar marker-pairs in all three lobes of the intact right lung when compared at the same transpulmonary pressure in the supine vs. prone positions.



**Figure 9** Comparison of distances between intra- and interlobar marker-pairs in the intact lungs of 3 dogs at total lung capacity (TLC) with each dog in the supine (ordinate) and prone (abscissa) body positions.

The close correspondence of distances between intralobar marker-pairs indicates again that each lobe in the intact thorax was not only at the same volume, but was expanded in a similar manner when the animal was in the prone and supine positions.

In contrast to intralobar intermarker distances, distances between interlobar marker-pairs (Figure 9), i.e., marker-pairs that span fissures, do not show the same high degree of linear correlation (range:  $r = 0.77$  to  $0.86$ ) that was observed with the intralobar marker-pairs. These data suggest, therefore, that individual lobes shift their positions relative to each other when the position of the animal is changed from the prone to the supine. Slippage of lobes along interlobar fissures could aid the lung in conforming to differing thoraco-abdominal configurations and shifts in thoracic



contents associated with postural changes without compromising regional expansion of the individual lung lobes.

INTERMARKER DISTANCES AT TLC IN  
ANESTHETIZED vs. ANESTHETIZED-PARALYZED DOG  
(Nembutal, Pavulon,  $P_{tp} = 25 \text{ cm H}_2\text{O}$  at TLC)

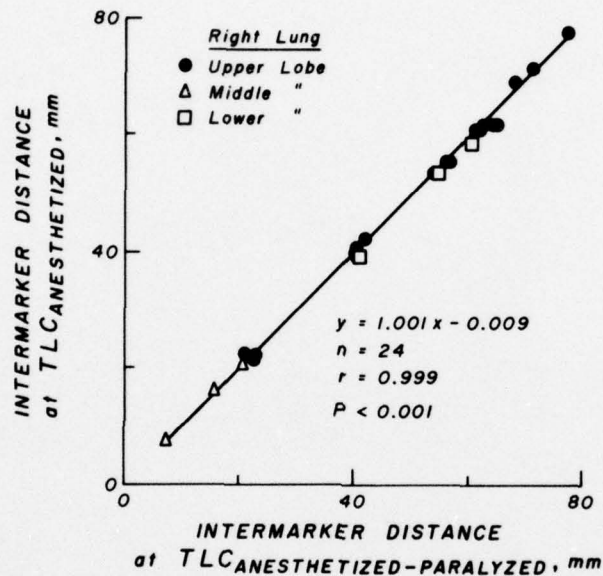


Figure 10 Comparison of distances between intralobar marker-pairs in the intact lung at total lung capacity in an anesthetized dog before (ordinate) and after (abscissa) muscle paralysis.

Initial studies in one dog indicate that regional lung expansion at TLC is the same in the anesthetized-paralyzed as in the anesthetized dog (Figure 10) which suggests that regional lung and chest wall geometries are not significantly altered by muscle paralysis.

Thus, we have observed a highly significant linear correlation of distances between intralobar marker-pairs in all three lobes of the right lung in the intact thorax of anesthetized dogs in the prone and supine positions at 25 cm H<sub>2</sub>O transpulmonary pressure. A similarly significant linear correlation was observed when the lung in the intact thorax was compared with the excised lung also at the same transpulmonary pressure (i.e.,  $P_{tp} = 25$  cm H<sub>2</sub>O). These data, therefore, indicate that regional lung expansion at total lung capacity is identical in intact dogs in the supine and prone positions and in individual lobes of the excised lung.

Generally, regional lung volumes are expressed as a percentage of regional volume at TLC. It is presumed that at TLC, all regions of the lung are expanded equally. Morphometric studies of lungs of dogs quick frozen at high inflation pressures ( $P_{tp} = 30$  cm H<sub>2</sub>O) revealed no systematic regional differences in alveolar size (6). In addition, Hogg and Nepszy (7) examined lung tissue density in dogs frozen head-up at TLC ( $P_{tp} = 30$  cm H<sub>2</sub>O) and found that regional volumes are reasonably uniform at TLC except for the extreme upper and lower lung regions. We are aware of no previous studies of regional lung expansion in the intact thorax of living (i.e., anesthetized) dogs with direct comparisons in the same lungs after removed from the thorax.

The results reported here indicate that regional lung expansion at TLC, defined in these studies as that lung volume obtained when  $P_{tp} = 25$  cm H<sub>2</sub>O, appears to be identical in dogs with an intact thorax in both the supine and prone body positions and in the individual lobes of the excised lung. If we assume that excised lungs are uniformly expanded at TLC because, at high inflation pressure, and in the presence of a uniform pleural pressure, they are too stiff to be deformed by their own weight, then we can conclude that at TLC, regional lung expansion is uniform or isotropic in the dog with an intact thorax. This follows from the



fact that since the parenchymal markers were randomly distributed throughout the lung, the close agreement in intralobar intermarker distances, intact and excised, indicates that the lungs were also uniformly expanded in the intact thorax. Therefore, in analyses of regional lung deformation, changes in lung parenchymal shape and dimensions from those pertaining at TLC represent changes from the state of uniform or isotropic expansion. This does not mean that overall lung shape intact and excised was the same or even that thoracic cavity shape at TLC in the supine vs. prone animal was necessarily the same. But the data do show that at TLC, while overall lung shape may be different in different body positions, individual lobes remain uniformly expanded and could presumably accommodate different thoracic shapes by altering their positions relative to each other.

Part II: Finite-Element Analysis of Strain Variations in an Excised Lobe of the Canine Lung

Experimental Preparation. A 10-kg dog was anesthetized with an intravenous injection of sodium pentobarbital (30 mg/kg) and the right lower lobe of the lung was excised via a median sternotomy. The lobe was rinsed with physiologic saline and kept moist throughout the experiment by spraying lightly with saline at frequent intervals. Metallic markers, consisting of 1-mm diameter spheres and cylindrical rods of 2-mm in length were affixed to the pleural surface of the excised lobe. The upper-half panels of Figure 11 shows two photographs of the excised lobe in the position which it was studied and viewed from front and rear, respectively. A three-dimensional drawing of the lobe depicting the positions of the markers is shown in the lower-half panel of Figure 11.

To inflate the lobe, a cannula (6-mm inside diameter) was inserted into the main bronchus of the lobe and tied securely in place. Airway pressure was measured with a water manometer connected via a Y-tube to the cannula. The transpulmonary pressure,

$P_{tp}$ , of the lobe was then equal to the airway pressure since pleural pressure was equal to ambient pressure, except at the base where the weight of the lobe was supported.

EXCISED LOBE OF CANINE LUNG WITH  
INTRAPARENCHYMAL AND  
SURFACE METALLIC MARKERS  
(Dog, 10 kg, Right Lower Lobe)

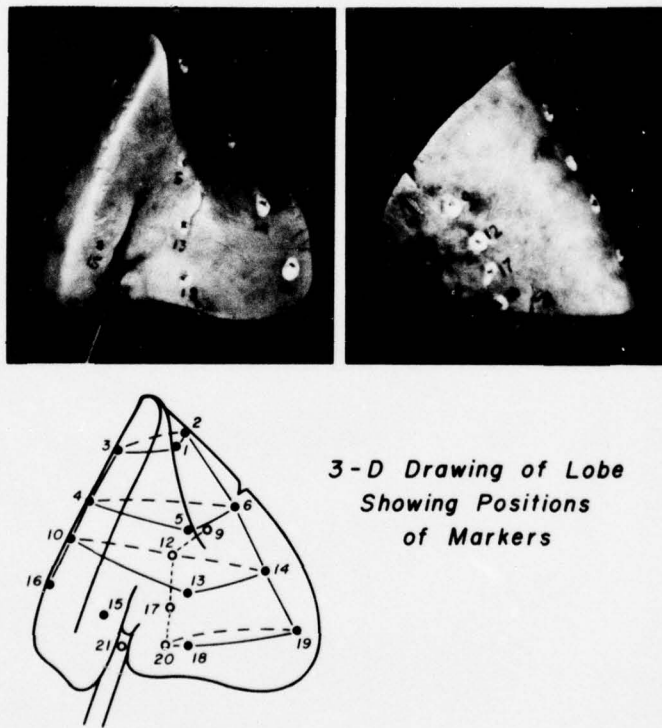


Figure 11 Upper-half: Photographs of excised right lower lobe of canine lung with intraparenchymal and surface metallic markers. Lower-half: Three-dimensional drawing of lobe showing spatial locations of the markers.

Static pressure-volume (P-V) maneuvers were performed with the lobe in the position shown in Figure 11, by manually inflating the lobe from  $P_{tp} = 4$  cm  $H_2O$  to total lobe capacity ( $TL_{OC}$ ), defined as  $P_{tp} = 20$  cm  $H_2O$ , and then deflating back to  $P_{tp} = 4$  cm

H<sub>2</sub>O in a stepwise manner (50 ml/volume change) Biplane roentgen-videographic images of this P-V maneuver were recorded on videotape, transferred to a stop-action video disc and the spatial (i.e., three-dimensional) coordinates of the markers were determined at each volume as described in Part I (above) and previously (2).

The three-dimensional coordinates of the metallic markers, relative to an arbitrary cartesian coordinate system are presented in Table 1 (see page 26). Four lobe volumes were studied beginning with TL<sub>O</sub>C ( $P_{tp} = 20$  H<sub>2</sub>O) followed by 80%, 60%, and 40% of TL<sub>O</sub>C at which time  $P_{tp}$  was equal to 4 cm H<sub>2</sub>O.

Formation of Tetrahedral Elements. A solid of complicated geometry to be analyzed by the finite-element technique has to be divided into a finite number of non-overlapping elements of simple shape (11). The most basic shape of elements hitherto used in three-dimensional finite-element analysis is a tetrahedron. The partitioning of the excised right lower lobe of canine lung into non-overlapping tetrahedrons can be implemented by selecting the metallic markers affixed to the pleural surface of the lobe as vertices to be shared by adjoining tetrahedrons. The step-by-step partitioning procedures are illustrated in Figures 12 and 13.

First, the lobe under consideration is approximated by the model displayed at the upper left corner of Figure 12 consisting of a space bounded by the four lines 1-5-13-18, 2-6-14-19, 2-9-12-20, and 3-4-10-16 connecting the selected metallic markers. The model is then partitioned into two regions, A and B, by use of the triangular cutting planes 1-2-9, 1-5-9, 5-9-13, 9-12-13, 12-13-20, and 13-18-20. Most of the major bronchi are contained in region A whereas region B is composed mostly of alveoli. Such partitioning thus allows the analysis of two regions with rather contrasting anatomic properties. To facilitate the analysis of strain variations during deflation of the lobe in the direction of the vertical body axis, regions A and B are both further



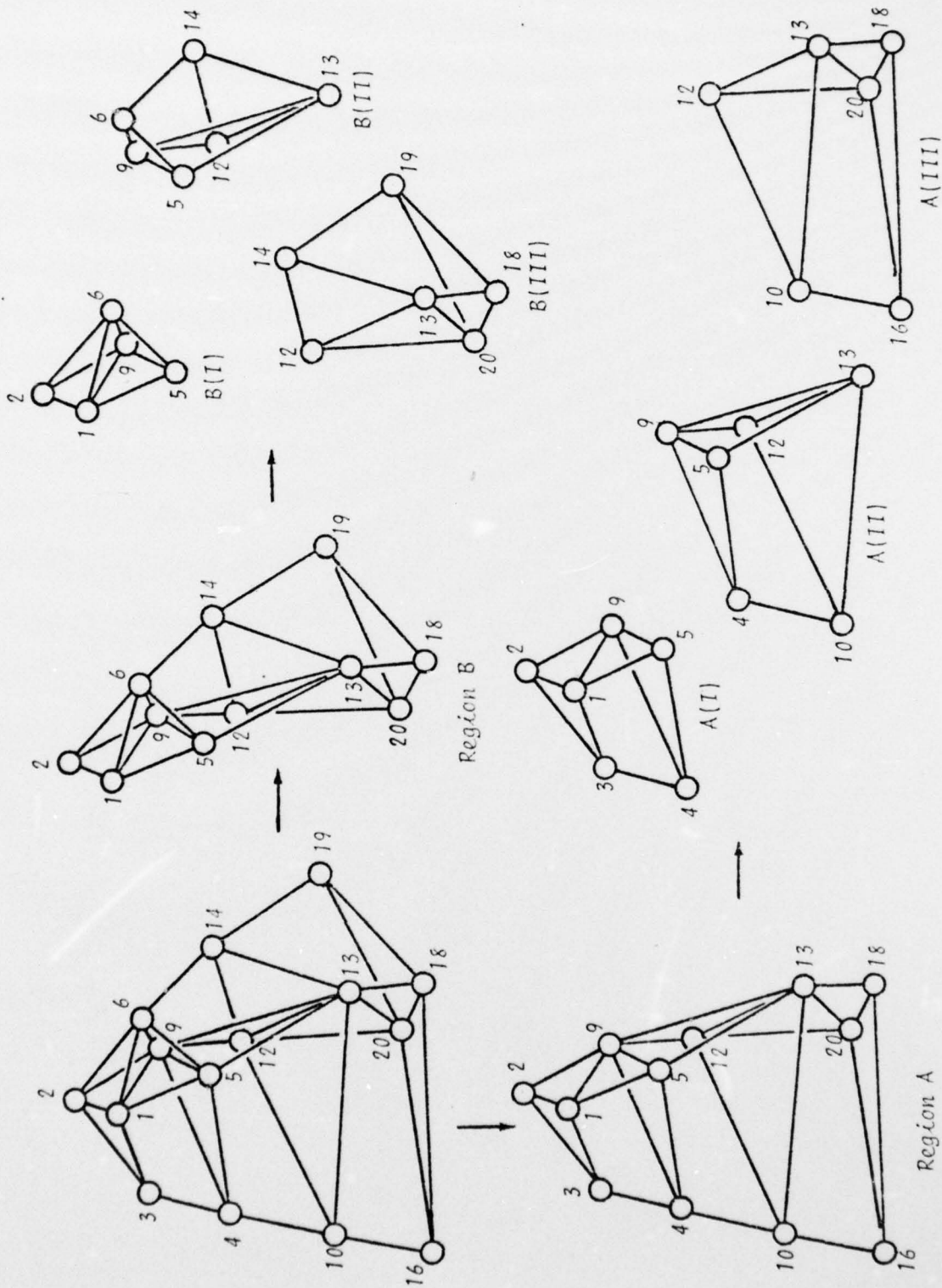
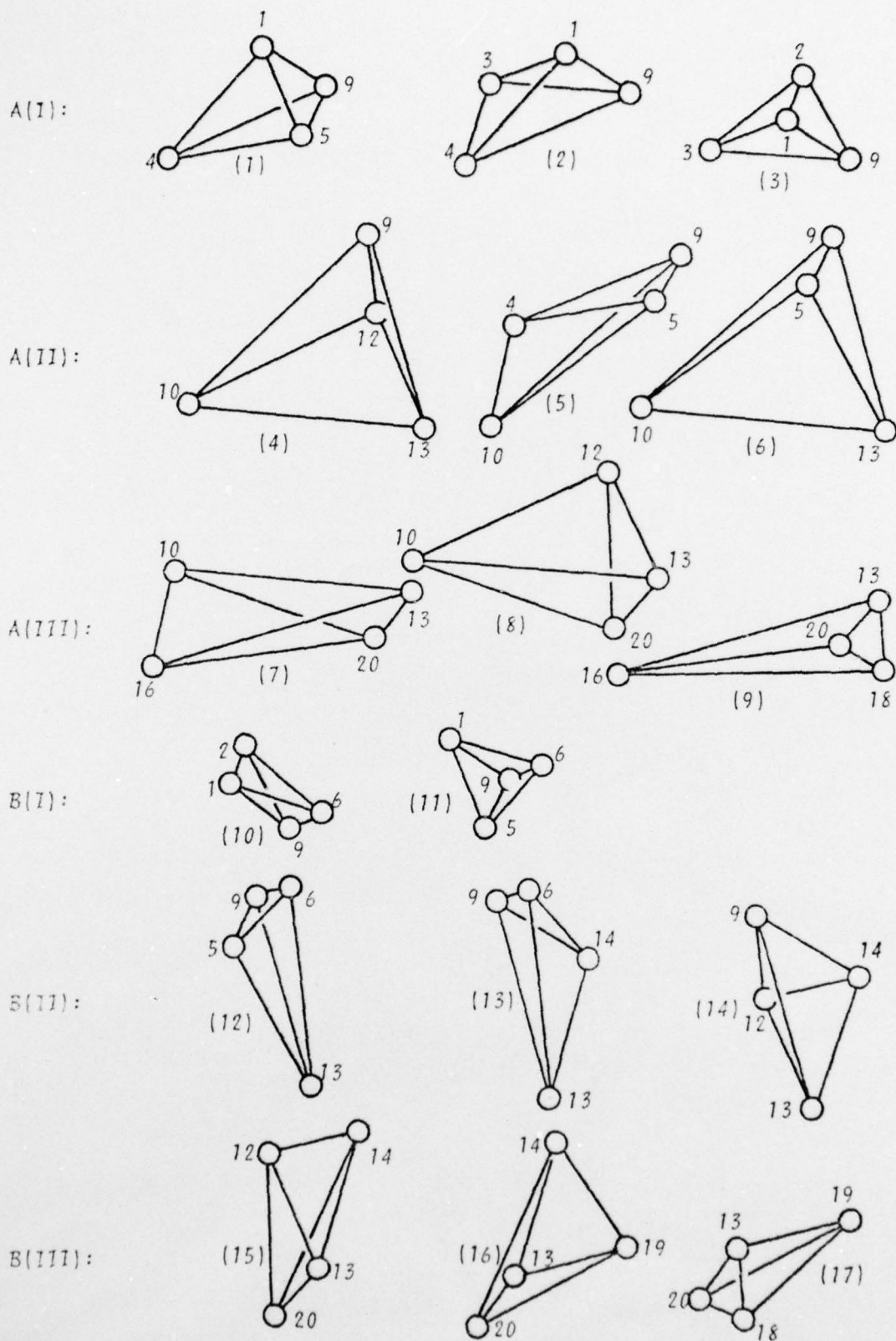


Figure 12 Partitioning of the excised right lower lobe into two regions A (left) and B (right), and each region into three layers I (upper), II (middle) and III (lower).



**Figure 13** Formation of 17 tetrahedrons from the 6 regions of the excised right lower lobe defined in Figure 12.

Table 1. Changes in the three-dimensional coordinates of the metallic markers shown in Fig. 1, recorded by biplane videoröntgenographic technique. (units are in cm. x 100).

Marker Number	100% TL <sub>0</sub> C			80% TL <sub>0</sub> C			60% TL <sub>0</sub> C			40% TL <sub>0</sub> C		
	x	y	z	x	y	z	x	y	z	x	y	z
1	-245	44	488	-231	15	427	-239	0	354	-283	0	251
2	-530	160	449	-507	118	388	-491	86	317	-522	82	202
3	-400	-175	428	-366	-183	358	-367	-184	279	-402	-169	184
4	-393	-300	218	-370	-291	171	-355	-282	105	-368	-256	28
5	-94	99	178	-81	86	142	-91	71	91	-135	65	31
6	-435	379	137	-417	341	107	-406	300	60	-425	272	-19
7	-539	269	127	-513	232	95	-489	197	46	-492	179	-39
8	-395	115	79	-378	98	52	-365	85	5	-367	72	-63
9	-501	235	61	-548	200	34	-523	172	-6	-514	145	-89
10	-394	-388	54	-373	-371	23	-359	-346	-19	-361	-317	-78
11	-425	66	-51	-403	54	-70	-381	36	-107	-380	29	-167
12	-539	113	-84	-518	92	-103	-493	73	-136	-481	62	-202
13	-51	114	-66	-30	101	-86	-37	88	-111	-71	81	-142
14	-212	508	-68	-210	478	-86	-212	438	-108	-234	395	-152
15	40	-275	-104	34	-269	-124	26	-266	-145	-11	-252	-166
16	-406	-434	-154	-373	-432	-165	-339	-430	-189	-312	-412	-218
17	-517	73	-205	-494	61	-214	-477	49	-239	-449	35	-282
18	115	94	-227	115	94	-239	100	89	-248	81	83	-260
19	58	611	-239	56	589	-245	32	559	-252	8	518	-274
20	-452	39	-332	-437	34	-341	-419	27	-345	-395	20	-364
21	-456	-123	-305	-444	-123	-311	-421	-121	-323	-405	-116	-351



divided into three layers, I (upper), II (middle), and III (lower) by use of the triangular cutting planes 4-5-9 and 10-12-13 for region A and, 5-6-9 and 12-13-14 for region B.

Three tetrahedral elements are then formed in each layer except the layer I of region B for which only two tetrahedral elements can be formed. This results in a total of seventeen tetrahedral elements, of which the numbering and their respective vertices are delineated in Figure 13.

Calculation of Normal and Shearing Strains. For evaluation of the strains in the lobe during the time interval of  $\Delta t = t' - t$ , the spatial coordinates of the implanted markers recorded at the instants  $t$  and  $t'$  can be utilized. The three-dimensional displacement of any point  $P$  in a tetrahedron formed with four implanted markers as vertices can be assumed as linear functions of its coordinates:

$$u_P = \alpha_1 + \alpha_2 x_P + \alpha_3 y_P + \alpha_4 z_P \quad v_P = \beta_1 + \beta_2 x_P + \beta_3 y_P + \beta_4 z_P \quad (1a,b,c)$$

$$w_P = \gamma_1 + \gamma_2 x_P + \gamma_3 y_P + \gamma_4 z_P$$

Since the displacements of the four vertices of the tetrahedron must also satisfy the above equations, it leads to twelve equations which suffice to solve for the twelve unknown coefficients  $\alpha$ 's,  $\beta$ 's, and  $\gamma$ 's. The results are, for  $i=1,2,3,4$

$$\alpha_i = \frac{1}{6V} \sum_{k=1}^4 C_{ki} u_k; \quad \beta_i = \frac{1}{6V} \sum_{k=1}^4 C_{ki} v_k; \quad (2a,b,c)$$

$$\gamma_i = \frac{1}{6V} \sum_{k=1}^4 C_{ki} w_k$$

where  $V$  is the volume of the tetrahedron equal to one sixth of the determinant of the matrix

$$M = \begin{bmatrix} 1 & x_1 & y_1 & z_1 \\ 1 & x_2 & y_2 & z_2 \\ 1 & x_3 & y_3 & z_3 \\ 1 & x_4 & y_4 & z_4 \end{bmatrix} \quad (3)$$

and  $C_{ki}$  in Equations (2) are the cofactors of the matrix  $M$  which is composed of the spatial coordinates of the four vertices of the tetrahedron.

It is well known from the theory of elasticity that the normal strains  $\epsilon$  and shearing strains  $\gamma$  are related to the displacements  $u$ ,  $v$ , and  $w$  by the equations

$$\begin{aligned} \{\epsilon\} &= [\epsilon_x \epsilon_y \epsilon_z \gamma_{xy} \gamma_{yz} \gamma_{zx}]^T \\ &= \left[ \frac{\partial u}{\partial x} \frac{\partial v}{\partial y} + \frac{\partial w}{\partial z} \frac{\partial v}{\partial x} + \frac{\partial u}{\partial y} \frac{\partial w}{\partial y} + \frac{\partial v}{\partial z} \frac{\partial u}{\partial z} + \frac{\partial w}{\partial x} \right]^T \end{aligned} \quad (4)$$

In Equations (3) and (4), the notation  $\{\}$  and  $[\ ]$  are used for vector and matrix, respectively, and  $T$  denotes the transposition of a matrix. Since the displacements are assumed to be linear functions of the spatial coordinates in Equation (1a,b,c), the strains obtained by partial differentiation of the displacements are therefore independent of the coordinates. The strains

so calculated represent the average values in the entire tetrahedron. Substitution of Equations (1) and (2) into Equations (4) gives the required formula for the strain calculations. That is

$$\{\epsilon\} = [B]\{\delta\} \quad (5)$$

where

$$\{\delta\} = [u_1 \ v_1 \ w_1 \ u_2 \ v_2 \ w_2 \ u_3 \ v_3 \ w_3 \ u_4 \ v_4 \ w_4]^T \quad (6)$$

$$[B] = [B_1 \ B_2 \ B_3 \ B_4] \quad (7)$$

and for  $i=1,2,3,4$

$$[B_i] = \begin{bmatrix} C_{i2} & 0 & 0 & C_{i3} & 0 & C_{i4} \\ 0 & C_{i3} & 0 & C_{i2} & C_{i4} & 0 \\ 0 & 0 & C_{i4} & 0 & C_{i3} & C_{i2} \end{bmatrix}^T \quad (8)$$

Hence, the procedure of calculating the normal and shearing strains is first to construct the matrix  $M$  and then compute its cofactors  $C_{ij}$  to form the matrix  $B$ , and finally use Equation (5). Not only are the spatial coordinates of the four vertices of the tetrahedron at the last instant  $t'$  required, but also the changes in their spatial coordinates are needed for the calculation of strains. The next section discusses how the displacements of a tetrahedral element's vertices are to be calculated based on the changes in their spatial coordinates.

Engineering Strains and Instantaneous Strains. Suppose that the spatial coordinates of the implanted markers are recorded at instants  $t = t_1, t_2, \dots, t_n$ . Any one of these instants can be chosen as the reference frame,  $t_r$ . Both the engineering strains and instantaneous strains of the tetrahedron can be computed.



Engineering strains are determined using Equation (5) with the displacements calculated at instant  $t_j$  as follows:

$$u_i = x_i(t_j) - x_i(t_r) \quad v_i = y_i(t_j) - y_i(t_r) \quad (9a,b,c)$$

$$w_i = z_i(t_j) - z_i(t_r)$$

Equations (9) are to be used for  $i=1,2,3,4$  to correspond to the four vertices of the tetrahedron.

Instantaneous strains at instant  $t_j$  are determined using Equation (5) and the spatial coordinates of the vertices at two consecutive instants  $t_{j-1}$  and  $t_j$ . The displacements are computed with equations, for  $i=1,2,3,4$

$$u_i = x_i(t_j) - x_i(t_{j-1}) \quad v_i = y_i(t_j) - y_i(t_{j-1}) \quad (10a,b,c)$$

$$w_i = z_i(t_j) - z_i(t_{j-1})$$

Numerical Results and Discussion. Based on the data presented in Table 1 of the changes in the spatial coordinates of metallic surface markers recorded during deflation of an excised lobe of canine lung, the engineering (cumulative) normal and shearing strains calculated by the finite-element method are presented in Tables 2 and 3, respectively. These are region-by-region, tetrahedron-by-tetrahedron results. As mentioned above, the strain values determined by the tetrahedral-element approach represent the averages for all of the points contained in that tetrahedron. To improve the accuracy of the strain results, their values at the partitioning nodes (selected metallic markers) can be modified by averaging the respective strain values in

Table 2. Changes in engineering normal strains in the 6 regions and 17 tetrahedrons of the lobe during the deflating process.

Regions and Tetrahedron Numbers	100% + 80% TL <sub>0</sub> C			100% + 60% TL <sub>0</sub> C			100% + 40% TL <sub>0</sub> C		
	$\epsilon_x$	$\epsilon_y$	$\epsilon_z$	$\epsilon_x$	$\epsilon_y$	$\epsilon_z$	$\epsilon_x$	$\epsilon_y$	$\epsilon_z$
A(I)	1	-.03718	-.03528	-.07556	-.10590	-.15329	-.14051	-.20509	-.24385
	2	-.13338	-.08967	-.12253	-.14208	-.15780	-.20334	-.16239	-.24658
	3	-.04777	-.09430	-.08307	-.12149	-.17263	-.15843	-.15100	-.24023
A(II)	4	-.00251	-.07792	-.06115	-.06744	-.15948	-.11193	-.16023	-.24608
	5	-.04130	-.07554	-.10316	-.11683	-.15462	-.25493	-.21412	-.24116
	6	-.02906	-.07626	-.06530	-.09570	-.15926	-.17075	-.19347	-.24346
A(III)	7	.05750	.00646	-.09248	.06169	.02086	-.18135	.00989	-.01201
	8	-.00083	-.00015	-.04397	-.06656	-.16894	-.15200	-.15802	-.24396
	9	-.04194	-.03296	-.04405	-.09608	-.06318	-.13667	-.14151	-.11333
B(I)	10	-.04535	-.03921	-.03789	-.12973	-.13700	-.16930	-.19078	-.16692
	11	-.04651	-.04337	-.07599	-.11490	-.13189	-.15037	-.22330	-.17660
	12	-.04182	-.05239	-.06469	-.11132	-.14101	-.17038	-.21937	-.18202
B(II)	13	-.03903	-.03229	-.05320	-.10718	-.10031	-.16671	-.22064	-.17684
	14	-.00444	-.03501	-.05920	-.06972	-.09921	-.11464	-.16245	-.18682
	15	-.00131	-.03594	-.04189	-.06720	-.09915	-.15622	-.15856	-.18722
B(III)	16	.01210	-.03684	-.05427	-.05574	-.09415	-.13638	-.13005	-.17464
	17	-.04209	-.04129	-.04833	-.09722	-.08883	-.13990	-.14528	-.15559
									-.22491

Table 3. Change in engineering shearing strains in the 6 regions and 17 tetrahedrons of the lobe during the deflating process.

Regions and Tetrahedron Numbers		100% → 80% TL <sub>0</sub> C			100% → 60% TL <sub>0</sub> C			100% → 40% TL <sub>0</sub> C		
		Y <sub>xy</sub>	Y <sub>yz</sub>	Y <sub>zx</sub>	Y <sub>xy</sub>	Y <sub>yz</sub>	Y <sub>zx</sub>	Y <sub>xy</sub>	Y <sub>yz</sub>	Y <sub>zx</sub>
A(I)	1	.03481	-.03370	-.01030	.03017	-.01111	-.03842	-.03708	-.01969	-.02020
	2	-.01016	-.00179	.12424	-.00738	.02449	.07448	.02332	-.00101	-.01929
	3	-.03713	.00543	-.00007	.01741	.01128	.00855	.00386	.02172	-.04990
A(II)	4	.03526	-.01875	.06728	.04572	.00056	.06810	.04562	-.04927	.10355
	5	.03287	.00193	.01801	.04562	-.04339	.04395	.04697	-.03273	.04989
	6	.03495	.00643	-.03810	.03931	-.00004	-.05793	.04734	-.01452	-.04837
A(III)	7	-.12192	.04798	-.01077	-.27869	.17001	-.08809	-.37169	.20645	-.14228
	8	.02369	-.02264	.02170	.04083	-.04582	.04606	.02972	-.07029	.04870
	9	.01310	-.06592	.09232	-.01388	-.09073	.09865	-.06893	-.09365	-.00457
B(I)	10	-.00954	-.02060	-.01231	.00994	-.05996	-.02405	-.07037	.00786	-.07393
	11	-.00039	-.02348	-.02300	-.00779	-.04024	-.05779	-.03463	-.00981	-.04622
B(II)	12	-.00926	.01477	-.04197	-.01761	.00538	-.06359	-.03914	.01988	-.05214
	13	-.03684	-.02453	-.00174	-.05069	-.06196	-.02042	-.03169	-.00064	-.06342
	14	-.03070	-.05618	.12317	-.03211	-.04639	.13447	-.03012	-.08299	.16851
B(III)	15	-.03035	-.04275	.03771	-.03119	-.05215	.06763	-.03057	-.04130	-.06706
	16	-.02722	-.03605	.02362	-.01414	-.07726	.03683	.01227	-.11508	-.03626
	17	.01605	-.04162	.09045	.00611	-.06873	.09411	-.00552	-.07787	-.01650



all of the tetrahedrons which share the node under consideration. For example, node 1 is shared by the tetrahedrons (1), (2), (3), (10) and (11) as indicated in Figure 13. Thus, as far as  $\epsilon_x$  at node 1 during the first deflation step (the column of 100%  $\rightarrow$  80% TL<sub>0</sub>C in Table 2) is concerned, the values -.03718, -.13338, -.04777, -.04535, and -.04651 for the five sharing tetrahedrons can be combined to give an average value equal to -.06204. This process of averaging has been applied for all nodes and the results are presented in Table 4 (see page 34). For interpretation of the strain results, the data in Tables 2 and 3 are to be used for the strain changes at the centroids of the tetrahedrons, and Table 4 for those changes occurring at the nodes.

When  $\epsilon_x$  changes are plotted (Figure 14), it is observed that the lower layers of both regions A and B respond with smaller  $\epsilon_x$  than the other layers at the beginning stage of the volume decrease but tend to follow the general trend of the other layers at later stages of the deflation process. It is also noteworthy that the strain variations can also be studied around the surface of the lobe by traversing along the lines 1-5-13-18, 2-6-14-19, 2-9-12-20, and 3-4-10-16 which are the four partitioning lines used in the formation of the tetrahedrons. The information needed for such study can be extracted from Figure 14. For example, the strain data for the line 1-5-13-18 are those illustrated in the second column of each of Figures 14(a) through 14(h); the node-1 column of Figure 14(e) may also be considered as second column with the first and fourth columns unavailable.

Changes of  $\epsilon_y$  are found similar to those of  $\epsilon_x$ . The apex-to-base variations of strains,  $\epsilon_z$ , are generally greater in magnitude than  $\epsilon_x$  and  $\epsilon_y$ . And this disparity between the radial strains,  $\epsilon_x$  and  $\epsilon_y$ , and the axial strain,  $\epsilon_z$ , is more pronounced at the basal (lower) region than at the apical (upper) region of the lobe. Figure 15 shows the relatively uniform region-by-region and layer-by-layer  $\epsilon_z$  changes in the excised lobe.

Table 4. Changes in the average engineering strains at the nodes  
(metallic markers) during the deflation process.

Node No.	% TL <sub>0</sub> C	$\epsilon_x$	$\epsilon_y$	$\epsilon_z$	$\gamma_{xy}$	$\gamma_{yz}$	$\gamma_{zx}$
1	100→80	-.06204	-.07037	-.08901	-.00448	-.01483	.01571
	100→60	-.12282	-.15052	-.16439	.00847	-.01511	-.00745
	100→40	-.18651	-.21484	-.25693	-.00815	-.00019	-.04191
2	100→80	-.04656	-.06676	-.08548	.02334	-.00759	-.00619
	100→60	-.12561	-.15482	-.16387	.01367	-.02434	-.00775
	100→40	-.17089	-.20358	-.25525	-.03326	.01479	-.06192
3	100→80	-.09058	-.09199	-.10280	-.02365	.00182	.06209
	100→60	-.13179	-.16522	-.18089	.00501	.01789	.04152
	100→40	-.15670	-.24341	-.26306	.01359	.01036	-.03460
4	100→80	-.07062	-.08350	-.10042	.01917	-.01119	.04398
	100→60	-.12160	-.15524	-.19959	.02280	-.01000	.02667
	100→40	-.19387	-.24386	-.29262	.03579	-.01781	.00347
5	100→80	-.03917	-.06657	-.07694	.01860	-.00681	-.01907
	100→60	-.10893	-.14801	-.17739	.01794	-.01788	-.03476
	100→40	-.21107	-.21742	-.28229	.01152	-.01137	-.02341
6	100→80	-.04293	-.04182	-.07044	-.01401	-.01346	-.01976
	100→60	-.11578	-.12755	-.16419	-.01654	-.03920	-.04146
	100→40	-.21352	-.17560	-.26016	-.04396	-.00432	-.05893
9	100→80	-.04249	-.06382	-.07743	.00035	-.01368	.01866
	100→60	-.10748	-.14241	-.16466	.00660	-.02013	.00612
	100→40	-.19117	-.21369	-.25938	-.00016	-.01465	-.00468
10	100→80	-.00324	-.06068	-.07312	.00097	.00299	.01162
	100→60	-.05697	-.12429	-.17419	-.02144	.01626	.00242
	100→40	-.14319	-.19733	-.29147	-.04041	.00793	.00230
12	100→80	-.00227	-.05746	-.05155	-.00053	-.03508	.06247
	100→60	-.06773	-.13170	-.13370	-.00581	-.03595	.07905
	100→40	-.15982	-.21602	-.25619	-.00366	-.06096	.09696
13	100→80	-.01204	-.04504	-.05714	-.01211	-.02175	.03306
	100→60	-.07022	-.10479	-.14881	-.02785	-.02428	.02871
	100→40	-.15270	-.17472	-.25750	-.03405	-.02903	.00221
14	100→80	-.00792	-.03552	-.05214	-.03128	-.03988	.04569
	100→60	-.07496	-.09821	-.14349	-.03203	-.05944	.05463
	100→40	-.16793	-.18138	-.25175	-.02003	-.06000	.03397
16	100→80	.00778	-.01325	-.06827	-.05441	-.00897	.04078
	100→60	-.01720	-.02116	-.15901	-.14629	-.03964	.00528
	100→40	-.06581	-.06267	-.27367	-.22031	-.05640	-.07343
18	100→80	-.04202	-.03713	-.04619	.01458	-.05377	.09139
	100→60	-.09665	-.07601	-.13829	-.00389	-.07973	.09638
	100→40	-.14340	-.13446	-.22418	-.03723	-.08576	-.01054
19	100→80	-.01500	-.03907	-.05130	-.00559	-.03884	.05704
	100→60	-.07648	-.09149	-.13814	-.00402	-.07300	.06547
	100→40	-.13767	-.16512	-.22511	.00338	-.09648	-.02638
20	100→80	-.00276	-.03679	-.05417	-.02111	-.02683	.04251
	100→60	-.05352	-.08223	-.15042	-.04849	-.02745	.04253
	100→40	-.12059	-.14779	-.26996	-.07245	-.03196	-.01398

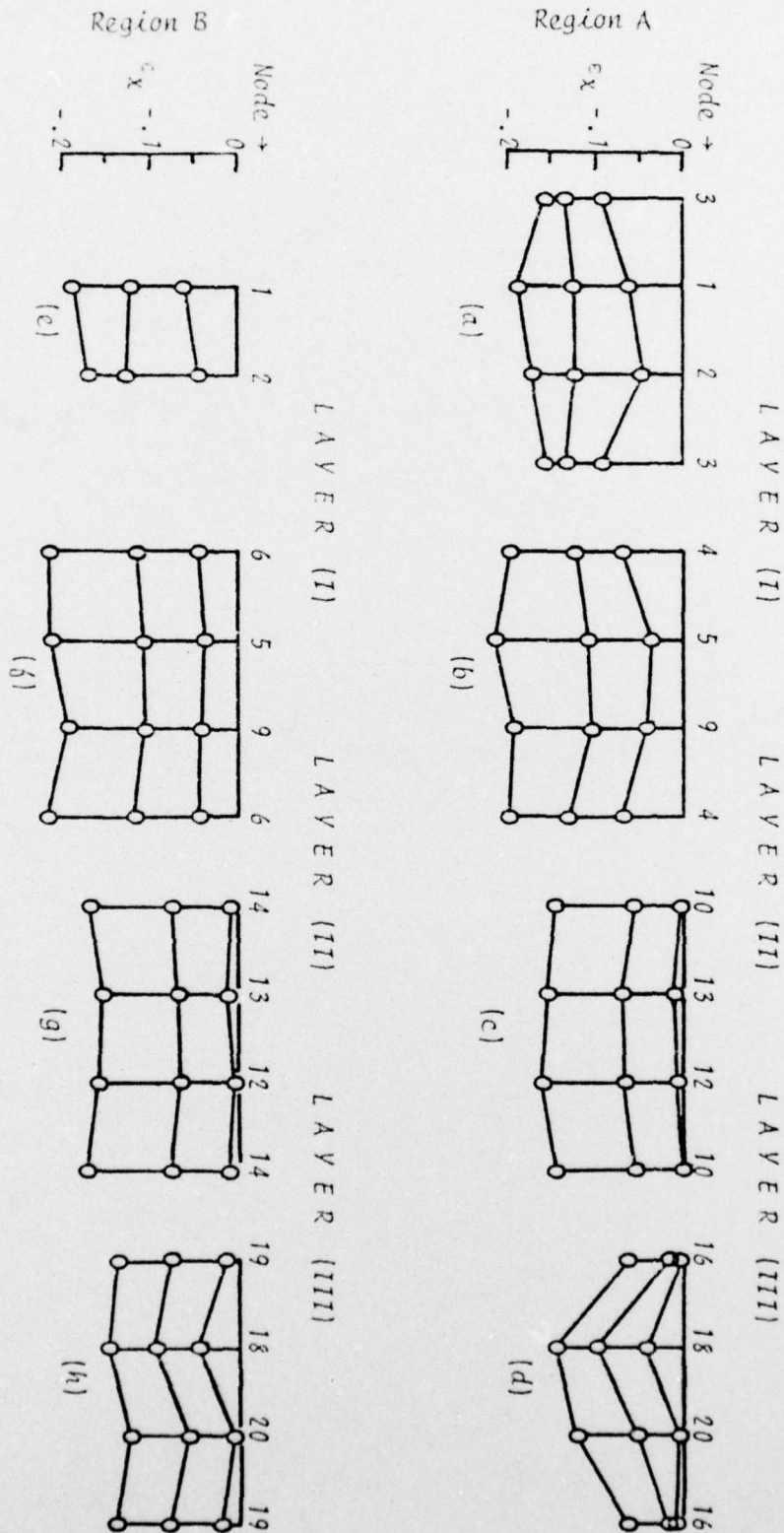


**Figure 14** Comparison of the changes of the normal strain in the x-direction during the deflation process of the excised lobe.



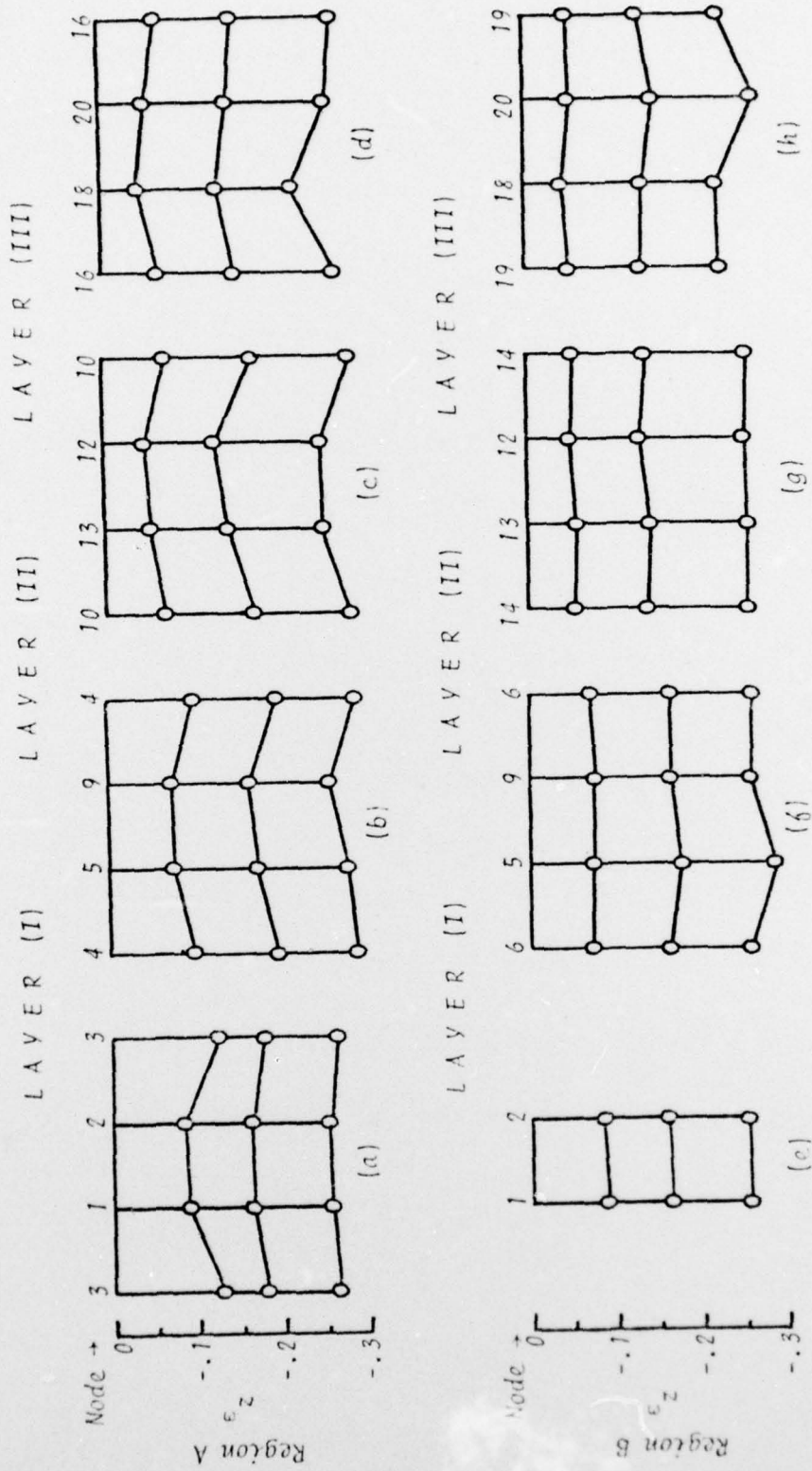


Figure 15 Comparison of the changes of the normal strain in the z-direction during the deflation process of the excited lobe.

As shown in Table 4 and Figure 16, the shearing strains are small as compared with the normal strains except in the vicinity of the node 16. The reason for such behavior of the lobe in this vicinity being different from other localities could be the nearness of this node 16 to the cannula which was inserted into the main bronchus of the lobe and held it securely during the deflation experiment.

The average strains in layers (I), (II), and (III), and in the regions A and B can be obtained by combining the strain data for the tetrahedral elements in the layers and the regions, respectively. The results are listed in Table 5. Generally speaking, region A exhibits greater normal strains but smaller shearing strains than region B, and the basal layer (III) exhibits smaller normal strains but greater shearing strains than the apical layer (I) in both regions A and B. Since region A and basal layers contain relatively more bronchi than region B and apical layers, such disparities in the strains during the inflation-deflation process might be expected.

Displacement functions other than those given in Equations (1) and large strain equations, instead of small strain equations (Equations (4)), are being studied so that the developed method can be expanded and applied not only for the excised lung lobes but also for the intact working lungs, and furthermore for the evaluation of the rotation and translation of the intact working lungs during various respiratory maneuvers and thoraco-abdominal configurations.

Table 5. Comparison of regional average engineering normal and shearing strains.

I. Average Normal Strains

REGIONS	100% + 80% TL <sub>0</sub> C			100% + 60% TL <sub>0</sub> C			100% + 40% TL <sub>0</sub> C		
	$\epsilon_x$	$\epsilon_y$	$\epsilon_z$	$\epsilon_x$	$\epsilon_y$	$\epsilon_z$	$\epsilon_x$	$\epsilon_y$	$\epsilon_z$
A(I)	-.07277	-.08975	-.09372	-.12315	-.16124	-.16742	-.17286	-.24358	-.25854
A(II)	-.02429	-.07657	-.07653	-.09332	-.15778	-.17920	-.18927	-.24356	-.27636
A(III)	.00491	-.03600	-.06016	-.03365	-.07042	-.15667	-.09655	-.12310	-.28389
Entire "A"	-.03072	-.06744	-.07680	-.08337	-.12981	-.16776	-.15289	-.20341	-.27293
B(I)	-.04593	-.04129	-.08194	-.12231	-.13444	-.16150	-.20702	-.17176	-.25450
B(II)	-.02809	-.04016	-.05903	-.09607	-.11351	-.15057	-.20082	-.18189	-.24647
B(III)	-.01043	-.03802	-.04816	-.07339	-.09404	-.14416	-.14463	-.17248	-.25602
Entire "B"	-.02815	-.03982	-.06304	-.09725	-.11400	-.15208	-.18416	-.17537	-.25233

II. Average Shearing Strains

REGIONS	100% + 80% TL <sub>0</sub> C			100% + 60% TL <sub>0</sub> C			100% + 40% TL <sub>0</sub> C		
	$\gamma_{xy}$	$\gamma_{yz}$	$\gamma_{zx}$	$\gamma_{xy}$	$\gamma_{yz}$	$\gamma_{zx}$	$\gamma_{xy}$	$\gamma_{yz}$	$\gamma_{zx}$
A(I)	-.00416	-.01002	.03795	-.01339	.00827	.01487	-.00330	.00034	-.02980
A(II)	.03436	-.00346	.01573	.04355	-.01447	.01804	.04664	-.03217	.03502
A(III)	-.02837	-.01352	.03441	-.08389	.01115	.01887	-.13697	.01417	-.03272
Entire "A"	.00061	-.00900	.02936	-.00898	.00663	.01726	-.02945	-.00589	-.00917
B(I)	-.00496	-.02204	-.01765	.00107	-.05010	-.04092	-.05250	-.00097	-.06007
B(II)	-.02560	-.02198	-.02648	-.03347	-.03432	.01682	-.03365	-.02125	-.01765
B(III)	-.01384	-.04014	.05059	-.01307	-.06604	.06619	-.00794	-.07808	-.03994
Entire "B"	-.01480	-.02805	.00215	-.01516	-.05015	.01403	-.03136	-.03343	-.02745



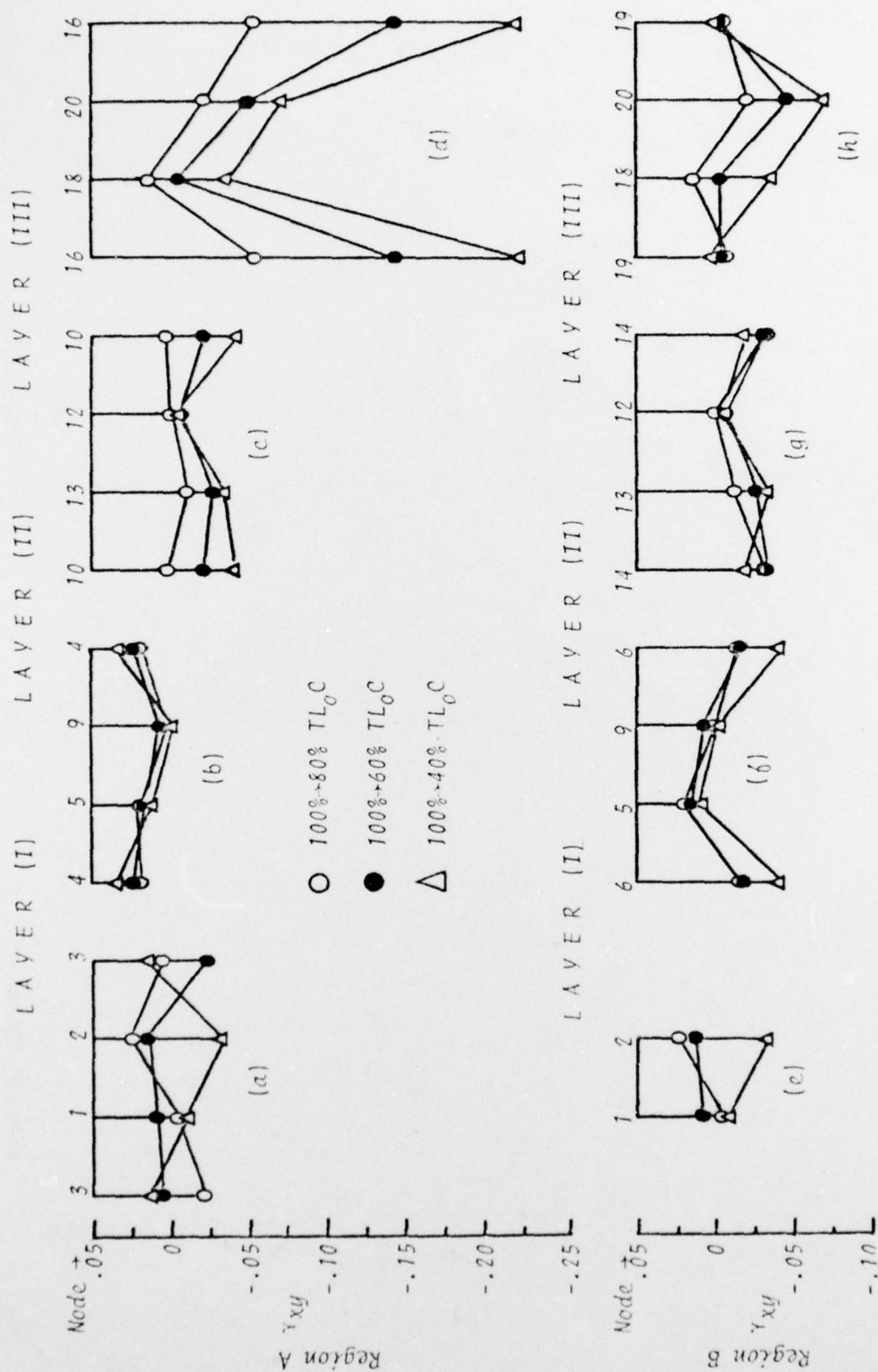


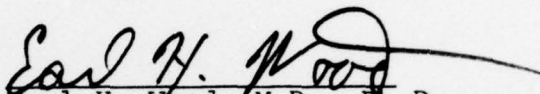
Figure 16 Comparison of the changes of the regional shearing strain in planes transverse to the z-axis,  $\gamma_{xy}$ , during the deflation process of the excised lobe.

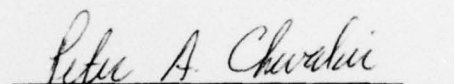
Overall Program Summary and Significance. The development in our laboratory of the parenchymal marker technique utilized in Parts I and II as well as the ability to reconstruct the three-dimensional shapes and dimensions of the heart, lungs, chestwall and diaphragm, in the intact thorax (detailed in last year's progress report) presents a unique opportunity to study dynamic regional lung mechanics and lung-chest wall-diaphragm interaction under various conditions of lung volumes and body position and thereby provides the methodology to study the effects on regional lung function of alterations in these parameters induced by changes in the gravitational-inertial force environment. The results described in Parts I and II represent significant new information regarding regional mechanical properties of the lung and clearly indicate the need to study the intrinsic elastic behavior of the lung and its relationship to the chest wall and diaphragm in the intact thorax with techniques possessing sufficient temporal and spatial resolution to permit quantitative determination of the dynamic changes in spatial (three-dimensional) lung parenchymal strains, regional lung volumes and lung-chest wall geometries.

Mechanical studies of the intact lung have, heretofore, not been possible. These data, which cannot be obtained by other methods, provide a quantitative measure of the mechanical properties of the lung under normal physiologic conditions (i.e., an intact thorax and normal intrathoracic pressures) at 1G and are required before any similar studies can be performed under conditions of increased or decreased gravitational-inertial force environments encountered in aerospace flight.

Because of the very large differences in specific gravity of the air in the alveoli, and the lung parenchyma and its mobile blood content plus the anatomically fragile nature of the lungs, the respiratory system is the most susceptible of all bodily organs to malfunction and actual structural damage during exposure to changes in the direction and magnitude of the gravitational-inertial force environment.

Consequently, increased knowledge concerning the mechanical characteristics and dynamic three-dimensional geometry of the lung is a basic requirement for understanding the factors which determine man's reactions and tolerance to short and long term changes in the force environment such as encountered in conventional and high-G aircraft and in manned space flight.

  
Earl H. Wood, M.D., Ph.D.  
Project Director

  
Peter A. Chevalier, Ph.D.  
Principal Investigator

November 23, 1977



References

1. Chevalier, P. A., L. D. Harris, J. F. Greenleaf, and R. A. Robb: Dynamic regional lung strains in awake dogs. *Physiologist* 18:168, 1975.
2. Chevalier, P. A., J. F. Greenleaf, R. A. Robb, and E. H. Wood: Biplane videoroentgenographic analysis of dynamic regional lung strains in dogs. *J Appl Physiol* 40:118-122, 1976.
3. Engel, L. A., H. Menkes, L. D. H. Wood, G. Utz, J. Joubert, and P. T. Macklem: Gas mixing during breath studied by intrapulmonary gas sampling. *J Appl Physiol* 35:9-17, 1973.
4. Fukuchi, Y., M. Cosio, S. Kelly, and L. A. Engel: Influence of pericardial fluid on cardiogenic gas mixing in the lung. *J Appl Physiol* 42:5-12, 1977.
5. Gillespie, D. J., Y. L. Lai, and R. E. Hyatt: Comparison of esophageal and pleural pressures in the anesthetized dog. *J Appl Physiol* 35:709-713, 1973.
6. Glazier, J. B., J. M. B. Hughes, J. E. Maloney, and J. B. West: Vertical gradient of alveolar size in lungs frozen intact. *J Appl Physiol* 23:694-705, 1967.
7. Hogg, J. C. and S. Nepszy: Regional lung volume and pleural pressure gradient estimated from lung density in dogs. *J Appl Physiol* 27:198-203, 1969.
8. Smith, H. C., J. F. Greenleaf, E. H. Wood, D. J. Sass, and A. A. Bove: Measurement of regional pulmonary parenchymal movement in dogs. *J Appl Physiol* 34:544-547, 1973.
9. Sturm, R. E., E. L. Ritman, R. J. Hansen, and E. H. Wood: Recording of multichannel analog data and video images on the same videotape or disc. *J Appl Physiol* 36:761-764, 1974.
10. Williams, J. C. P., R. E. Sturm, A. G. Taskiris, and E. H. Wood: Biplane videoangiography. *J Appl Physiol* 24:724-727, 1968.
11. Gallagher, R. H.: *Finite Element Analysis Fundamentals*. Prentice-Hall, New York. 1975.

Part III: Publications from this Laboratory Based on Work  
Performed Under and Supported by, this Contract (AF-  
49620-76-C-0001) for the Period 1976-1977:

All of the following publications acknowledge the support provided by this contract and the U. S. Air Force. Copies (3) of papers published during the past fifteen months (1976-1977) are included with this progress report. Copies of papers "In Press" will be forwarded upon receipt of reprints.

1. Robb, R. A., E. L. Ritman, J. F. Greenleaf, R. E. Sturm, H. K. Liu, P. A. Chevalier, and E. H. Wood: Quantitative imaging of dynamic structure and function of the heart, lungs and circulation by computerized reconstruction and subtraction techniques. SIGGRAPH 10(2):246-256 (March) 1976.
2. Johnson, S. A., R. A. Robb, E. L. Ritman, B. K. Gilbert, J. F. Greenleaf, L. D. Harris, M. J. Berggren, R. E. Sturm, P. A. Chevalier, R. M. Heethaar, E. H. Wood, G. T. Herman, and Y. C. Pao: Bioimage synthesis and analysis from x-ray, gamma, optical and ultrasound energy. In: Preston, K., Jr. and M. Onoe: Digital Processing of Biomedical Images. Plenum Press, New York, 1976, pp 203-226.
3. Gilbert, B. K., M. T. Storma, C. E. James, L. W. Hobrock, E. S. Yang, K. C. Ballard, and E. H. Wood: A real-time hardware system for digital processing of wideband video images. IEEE Transactions on Computers C25(11):1089-1100 (November) 1976.
4. Gilbert, B. K., M. T. Storma, K. C. Ballard, L. W. Hobrock, C. E. James, and E. H. Wood: A programmable dynamic memory allocation system for input/output of digital data into standard computer memories at 40 megasamples/second. IEEE Transactions on Computers C25(11):1101-1109 (November) 1976.
5. Gilbert, B. K., W. F. Sutterer, S. A. Johnson, R. E. Sturm, E. H. Wood, J. J. Tiemann, and R. D. Baertsch: A charge coupled transversal filter for biomedical signal conditioning. Instrument Society of America Transactions 15:169-174, 1976.
6. Johnson, S. A., J. F. Greenleaf, R. C. Bahn, W. F. Samayoa, F. Duck, C. Hansen, M. Tanaka, and A. Lent: Reconstruction of three-dimensional ultrasound tissue properties from transmission and other data. Proceedings of the Conference on Computerized Tomography in Radiology, American College of Radiology, St. Louis, Missouri, April 25-28, 1976, pp 149-162.

7. Wood, E. H. and E. L. Ritman: Zero reference and calibration problem of circulatory pressure recorded by implanted and indwelling pressure transducers, and a look at future technology for studies of dynamic relationships of structure to function of the heart, lungs, and circulation. In: Fleming, David G., Wen H. Ko, and Michael R. Neuman: Indwelling and Implantable Pressure Transducers. Cleveland, Ohio, CRC Press, Inc., 1977, pp 21-34.
8. Wood, E. H., E. L. Ritman, L. D. Harris, and P. E. Rueggsegger: New vistas for studies of structural and functional dynamics of the heart, lungs, and circulation by quantitative imaging. Proceedings, Conference on Diagnostic Imaging, Chicago, Illinois, September 27-28, 1976.
9. Johnson, S. A., E. L. Ritman, and E. H. Wood: A unique bio-image synthesis and analysis facility at Mayo Clinic. Proceedings, IEEE Systems, Man and Cybernetics Society, pp 244-245, 1977.
10. Robb, R. A., L. D. Harris, and E. L. Ritman: Computerized x-ray reconstruction tomography in stereometric analysis of cardiovascular dynamics. Proceedings of the Society of Photo-Optical Instrumentation Engineers 89:69-82, 1976.
11. Wood, E. H., D. J. Sass, E. L. Ritman, J. F. Greenleaf, C. M. Coulam, D. Nathan, and A. C. Nolan: Some effects of acceleration in man and chimpanzees. In: NASA Special Publication. Use of Non-Human Primates in Space, February, NASA CP-005, pp 103-164, 1977.
12. Wood, E. H., E. L. Ritman, R. A. Robb, L. D. Harris, and P. E. Rueggsegger: Noninvasive numerical vivisection of anatomic structure and function of the intact circulatory system using high temporal resolution cylindrical scanning computerized tomography. Medical Instrumentation 11(3):153-159, 1977.
13. Gilbert, B. K., W. F. Sutterer, J. J. Tiemann, S. A. Johnson, R. D. Baertsch, R. E. Sturm, and E. H. Wood: A charge coupled transversal filter for biomedical signal conditioning. Bio-medical Sciences Instrumentation, Instrument Society of America, Pittsburgh, Pennsylvania 12:51-56 (May) 1976.
14. Wood, E. H.: New vistas for the study of structural and functional dynamics of the heart, lungs, and circulation by noninvasive numerical tomographic vivisection. Dickinson Richards Memorial Lecture. Circulation 56:506-520 (October) 1977.
15. Ritman, E. L.: Quantitative transaxial imaging of the heart (review article). European Journal of Cardiology 5(3): 203-220, 1977.



16. Chevalier, P. A., R. A. Robb, L. D. Harris, J. F. Greenleaf, E. L. Ritman, and E. H. Wood: Dynamic spatial reconstruction tomography for quantitative studies of cardiopulmonary structure and function. Review of Air Force Sponsored Basic Research in Environmental and Acceleration Physiology, Wright-Patterson Air Force Base, Ohio, October 13-15, 1976.  
Abstract
17. Chevalier, P. A., J. R. Rodarte, and L. D. Harris: Regional lung expansion at total lung capacity (TLC) in intact vs. excised canine lungs. American Review of Respiratory Disease 115:314, 1977.  
Abstract
18. Rodarte, J. R., P. A. Chevalier, L. D. Harris, S. J. Lai-Fook, T. W. Wilson, and R. E. Hyatt: Regional parenchymal distortion in intact dogs. Symposium on "Stress Distribution in the Lungs." 1977, Paris, France.  
Abstract
19. Robb, R. A., E. L. Ritman, R. E. Sturm, and E. H. Wood: Computerized tomography of the heart: A system for dynamic three-dimensional imaging of cardiac structures and functions. 30th Annual Conference on Engineering in Medicine, November 5-9, 1977.  
Abstract
20. Chevalier, P. A., L. D. Harris, E. L. Ritman, and E. H. Wood: Regional lung expansion in the intact canine thorax in the prone and supine positions at 1G. 1977 Review of Air Force Sponsored Basic Research in Environmental and Acceleration Physiology, September 15-17, 1977, Galveston, Texas.  
Abstract
21. Wood, E. H.: The effects of transverse acceleration on chimpanzees. Proceedings of the "Use of Non-Human Primates in Space," NASA Ames Research Center, December 4, 1974 (In Press).
22. Ritman, E. L., R. E. Sturm, R. A. Robb, and E. H. Wood: Needs, requirements and design of a high temporal resolution synchronous cylindrical whole-body transaxial scanner for simultaneous study of the structure and function of the heart and circulation. In: Heintzen, P.: Roentgen Video Techniques for Dynamic Studies of Structure and Function. Stuttgart, Germany, G. Thieme, 1977 (In Press).
23. Sturm, R. E., E. L. Ritman, and E. H. Wood: Prototype of a single x-ray video imaging chain designed for a fully electronic, synchronous cylindrical scanning, dynamic spatial reconstruction system. In: Heintzen, P.: Roentgen Video Techniques for Dynamic Studies of Structure and Function. Stuttgart, Germany, G. Thieme, 1977 (In Press).

24. Wood, E. H. and E. L. Ritman: Current cat scanners in relation to the needs and requirements for a new generation high temporal resolution and high synchronous axial anatomic range and resolution dynamic spatial reconstruction system for simultaneous study of structure and functions of the heart and circulation. In: Heintzen, P.: Roentgen Video Techniques for Dynamic Studies of Structure and Function. Stuttgart, Germany, G. Thieme, 1977 (In Press)
25. Gilbert, B. K., A. Chu, and E. L. Ritman: Data management, computation, and display techniques for dynamic spatial reconstruction of structural and functional information from the heart, lungs and circulatory system. In: Heintzen, P.: Roentgen Video Techniques for Dynamic Studies of Structure and Function. Stuttgart, Germany, G. Thieme, 1977 (In Press).
26. Robb, R. A., L. D. Harris, P. A. Chevalier, and E. L. Ritman: Quantitative dynamic three-dimensional imaging of the heart and lungs by computerized synchronous cylindrical scanning reconstruction tomography. In: Heintzen, P.: Roentgen Video Techniques for Dynamic Studies of Structure and Function. Stuttgart, Germany, G. Thieme, 1977 (In Press).
27. Ruegsegger, P. E., L. D. Harris, S. W. Rowland, and E. L. Ritman: Predictions of the performance of a dynamic spatial reconstruction system based on mathematical simulations. In: Heintzen, P.: Roentgen Video Techniques for Dynamic Studies of Structure and Function. Stuttgart, Germany, G. Thieme, 1977 (In Press).
28. Harris, L. D., P. Ruegsegger, and E. L. Ritman: Computerized transaxial cross-sectional and cylindrical scanning of the structure and function of dynamic organs - the role of spatial and temporal resolution. In: Heintzen, P.: Roentgen Video Techniques for Dynamic Studies of Structure and Function. Stuttgart, Germany, G. Thieme, 1977 (In Press).
29. Smith, H. C., R. A. Robb, and E. L. Ritman: Roentgen video-densitometric assessment of myocardial blood flow: Clinical applications. In: Heintzen, P.: Roentgen Video Techniques for Dynamic Studies of Structure and Function. Stuttgart, Germany, G. Thieme, 1977 (In Press).
30. Robb, R. A., E. L. Ritman, L. D. Harris, and P. A. Chevalier: Dynamic spatial reconstruction tomography for quantitative studies of structure and function of the heart, lungs and circulation. Federation Proceedings, 1977 (In Press).
31. Wood, E. H., L. D. Harris, and P. E. Ruegsegger: Computerized three-dimensional reconstruction of structure and function of biologic objects. Federation Proceedings, 1977 (In Press).

32. Ritman, E. L., R. E. Sturm, R. A. Robb, and E. H. Wood: Quantitative multiaxial tomographic imaging of the heart, lungs and circulatory systems - physiologic requirements and implementation. Federation Proceedings, 1977 (In Press).
33. Greenleaf, J. F., H. C. Smith, P. A. Chevalier, D. J. Sass, A. A. Bove, and E. H. Wood: Effect of force environment on regional pulmonary displacements and volumes in dogs. Journal of Applied Physiology (In Press).
34. Ritman, E. L., H. C. Smith, R. A. Robb, R. E. Sturm, and E. H. Wood: Roentgen videodensitometry and video scanning densitometry application to the cardiovascular system. In: Carlsson, Erik: Cardiac Radiology. St. Louis, Missouri, C. V. Mosby (In Press).
35. Ritman, E. L., R. A. Robb, S. A. Johnson, P. A. Chevalier, B. K. Gilbert, J. F. Greenleaf, R. E. Sturm, and E. H. Wood: Quantitative imaging of the structure and function of the heart, lungs and circulation. Mayo Clinic Proceedings (In Press).
36. Ruegsegger, P. E., E. L. Ritman, and E. H. Wood: Performance of a cylindrical CT scanning system for dynamic studies of the heart and lungs. San Diego Biomedical Symposium (In Press).
37. Wood, E. H.: The why, uniqueness, how come and possible future of a dynamic spatial reconstructor at Mayo. (Editorial) Mayo Clinic Proceedings (In Press).
38. Gilbert, B. K., R. D. Beistad, E. E. Swartzlander, Jr., L. M. Krueger, A. Chu, R. D. Breuer, and E. L. Ritman: Development of very high-speed multi-axial tomographic algorithms employing digital high capacity fixed point arithmetic hardware. San Diego Biomedical Symposium (In Press).
39. Robb, R. A.: Three-dimensional dynamic imaging of the heart, lungs and circulation by roentgen-video computed tomography, "A comparison of modern imaging techniques for non-invasive medical dynamics," IEEE Seminar, Henniker, New Hampshire, August 15-20, 1976 (In Press).
40. Greenleaf, J. F., S. A. Johnson, and A. H. Lent: Measurement of spatial distribution of refractive index in tissues by ultrasonic computer assisted tomography. Ultrasound in Medicine and Biology (Submitted).
41. Swartzlander, E. E., B. K. Gilbert, and I. S. Reed: Inner product computers. IEEE Transactions on Computers (In Press).
42. Fellows, J. L., D. L. Cravath, M. A. Wondrow, E. L. Ritman, and H. C. Smith: Clinical laboratory techniques for computer-based analysis of cardiac roentgen angiograms. Analyzer (Submitted).



43. Chevalier, P. A. and J. R. Rodarte: Regional lung expansion at total lung capacity in intact vs. excised canine lungs. *Journal of Applied Physiology* (Submitted).
44. Chevalier, P. A., J. H. Reed, Jr., R. A. Vandenberg, and E. H. Wood: Effect of gravitational and inertial forces on vertical distribution of pulmonary blood flow. *Aviation, Space and Environmental Medicine* (In Press).
45. Pao, Y. C., P. A. Chevalier, J. R. Rodarte, and L. D. Harris: Finite-element analysis of strain variations in excised lobe of canine lung. *Journal of Biomechanics* (In Press).
46. Greenleaf, J. F., E. L. Ritman, P. A. Chevalier, D. J. Sass, and E. H. Wood: Spatial distribution of pulmonary blood flow in dogs in increased force environments. *Journal of Applied Physiology* (In Press).